UKAEA-CCFE-PR(19)70

J W Connor, R J Hastie, K Richards

On Energy Confinement following the Onset of 'Stiff ' Transport and the Effect of Radiation

On Energy Confinement following the Onset of 'Stiff ' Transport and the Effect of Radiation

J W Connor, R J Hastie, K Richards

This is a preprint of a paper submitted for publication in
Journal of Plasma Physics

On Energy Confinement following the Onset of 'Stiff' Transport and the Effect of Radiation

J W Connor [1, 2], R J Hastie [1] and K Richards[1, 3]

[1] CCFE, Culham Science Centre, Abingdon, Oxon OX 14 3DB, UK

[2] Department of Physics, Imperial College of Science and Technology and Medicine, London SW7 2BZ, UK

[3] Department of Physics & Astronomy, University College London, Gower Street, London WC 1E 6BT, UK

Abstract. For a tokamak plasma which encounters the onset of 'stiff transport' as the heating power increases, the determination of the radial extent of those stiff profiles and the resulting impact on energy confinement, is a subtle matter. The results depend on details of the heating profile and the transport model invoked. In this work we take a simple form for the heating profile, which has a variable width, together with a simple transport model, but allowing for several forms of the thermal diffusivity, to describe the non-stiff regions. This allows us to develop analytic solutions, leading to an energy confinement scaling law that takes account of stiff transport. Impurity radiative losses, which are anticipated to be necessary in a DEMO design, can also be considered in the model and the calculation is then used to quantify how much impurity radiation is permitted before the energy content starts to diminish.

1. Introduction

With increasing power input the temperature profiles in a tokamak plasma may well reach the threshold for the onset of ion or electron temperature gradient instabilities, predicted to lead to the sudden onset of a high level of energy transport. This essentially limits the gradient, a situation known as 'stiff' transport [Dimits *et al*., 2000, Suttrop *et al*., 1997]; i.e., there is no increase in the energy content with further increase in the input power. Indeed, modelling of energy confinement for the International Tokamak Experimental Reactor (ITER) being constructed at Cadarache in France anticipates this will be the case [ITER Expert Groups on Confinement and Confinement Modelling and Database, 1999, Doyle *et al*., 2007] and limits temperature gradients to this threshold value, known as the critical gradient. The plasma energy content is then simply calculated by assuming the input power suffices to achieve this threshold temperature profile at *all* radii. Because this criterion is in fact a condition on the logarithmic temperature gradient, the profile depends critically on the edge temperature. The base-line operational mode planned for ITER is the high confinement mode (H-mode) and this is given by the temperature at the top of the edge transport barrier and is known as the 'pedestal' temperature. However, as the input power increases towards the value needed for the fully stiff situation, only limited parts of the temperature profile will achieve the threshold value and the saturation of confinement with power is more gradual. A purpose of the present work is to explore this behaviour taking account of situations where different parts of the profile first experience the onset of stiffness.

A remarkable experimental result reported by ASDEX Upgrade is that the energy content of a discharge appears unchanged as the radiative losses increase [Ochoukov *et al*., 2015]. This is of importance for future fusion power plant designs [Kotschenreuther *et al*., 2007, Ward, 2010, Lux *et al*., 2015, Lux *et al*., 2016, Zohm *et al*., 2019 a, Zohm *et al*., 2019 b], where it appears necessary to introduce impurities to deliberately radiate a fraction of the lost power to limit damage from excessive heat fluxes on the surrounding structures. It has been proposed that this is a consequence of core transport being stiff as the radiative power increases, which has been supported by some transport modelling of burning plasma [Fable *et al.*, 2017]. We also investigate this further within the framework of our modelling above.

In general, determining the radial extent of the stiff profiles, using a transport code, as the heating increases is a subtle calculation, the results depending on details of the heating profile and the transport model. In this work we use a simple model for the heating profile and consider several forms of the thermal diffusivity in the 'non-stiff' regions. This allows us to develop analytic solutions, leading to an energy confinement scaling law that takes account of stiff transport and impurity radiative losses and, furthermore, can be used to quantify how much impurity radiation is permitted before the energy content starts to diminish.

As a first example, we assume that there is a net heating profile, $P(r)$, that is a constant, P, within a radius r_0 and zero beyond that (thus the total power is given by $P_{Tot} = 2\pi^2 P {r_0}^2 R$). The background thermal diffusivity, χ, is taken to be a constant in radius, χ_0. An edge boundary condition, $T = T_a$, on the temperature representing an edge H-mode pedestal is invoked. Thus, we are assuming that $P_{\rm Tot} > P_{\rm LH}$, the threshold power for the L-H confinement transition [ITER Expert Groups on Confinement and Confinement Modelling and Database, 1999, Doyle *et al*., 2007]. The effect on the power dependence of the energy confinement of including impurity radiative losses, $P_{\rm Rad}$ is accounted for by considering the effect P_{Rad} has on reducing the input power for a given value of the latter.

The effect of the onset of regions of stiff transport, characterised by a normalised critical temperature gradient parameter, $\hat{c} = ca/R$ (where the critical gradient is given by $\text{dln}T/\text{d}r = -c/R$), on the energy content of the plasma as a function of a normalised net heating power parameter $\lambda = \text{P}_{\text{Tot}}/n\chi_0 T_a$ is then calculated. Here n is the plasma density (taken to be constant in radius), R the major radius of the tokamak and a the minor radius, which allows us to introduce a normalised minor radius, $\rho = r/a$. This model is described in Section 2.

As mentioned above, the appearance of regions of stiff temperature profiles can become quite complicated, even for the simple model described above. We shall discover below that there are then two main cases to address: (i) $\hat{c}\rho_0 > 1$ (i.e., the heating profile is not too peaked) and (ii) $\hat{c}\rho_0 < 1$ (i.e., a more peaked heating profile), although this case actually splits into two sub-cases, (a) and (b), depending on whether $\rho_0 > \rho_{2\text{c}}$ or $\rho_0 < \rho_{2\text{c}}$, respectively. Here $\rho_{2\text{c}}$ is a critical radius dependent on $\hat{c}$ that controls whether stiffness sets in first at the plasma edge (case (a)), or an interior point (case (b)). These various situations are analysed in Section 3. In Section 4 we extend this model by assuming the thermal diffusivity is gyro-Bohm in nature, $\chi \propto T^{3/2}$. A refinement, in which an additional, radially increasing factor is inserted into χ in order to be more realistic, is considered in the Appendix.

This approach is reminiscent of earlier work exploring the impact on energy confinement of the onset of ideal ballooning modes [Connor *et al*., 1984].

Using the results for the energy content as calculated for the various cases above, we can obtain the energy confinement as a function of input power and infer the impact of radiative losses on the performance of the device. These results are presented in Section 5.

Finally, in Section 6 we summarise and discuss our results. Especially, we consider the implications of our results for describing the variation of tokamak confinement with heating power. Assessments of tokamak performance, particularly that of ITER, are often based on simple power-like scaling laws for energy confinement as a function of plasma and machine parameters, particularly input heating power, which do not recognise the possible appearance of a different regime associated with the onset of stiff behaviour. We propose a more complicated algebraic form for the energy confinement that fits our numerical calculations.

2. A Simple Transport Model

We describe the temperature profile by a simple transport equation:

$$\frac{1}{r}\frac{\mathrm{d}}{\mathrm{d}r}\left(rn\chi\frac{\mathrm{d}T}{\mathrm{d}r}\right) = -P_{\mathrm{H}} + P_{\mathrm{Rad}} \equiv -P \qquad , \tag{1}$$

where P_{H} is the input power density and P_{Rad} the radiative loss power density, so that P is the net heating power density. We first consider $P_{\mathrm{H}}, P_{\mathrm{Rad}}$, n, and χ to be constant in r. P is taken to be constant within a radius r_0 and zero outside:

$$P = P_0, \quad r < r_0; \quad P = 0, \quad r > r_0 \quad . \tag{2}$$

Thus

$$\frac{\mathrm{d}T}{\mathrm{d}r} = -\frac{1}{rn\chi_0}\int_0^r Pr\mathrm{d}r \;, \tag{3}$$

increases radially outwards. Should it arrive at a radius where it reaches the critical gradient condition, then the temperature profile becomes ‘stiff’ and eqn. (3) is replaced by:

$$\frac{1}{T}\frac{\mathrm{d}T}{\mathrm{d}r} = -\frac{c}{R} \;, \tag{4}$$

with the number c in the range 4 to 6. As we shall see below, this may occur at several radial points.

To calculate the plasma energy content and confinement time, τ_E, we define

$$W = \frac{3}{2}n\int_0^a Tr\mathrm{d}r\,; \quad \tau_E = \frac{3}{2}n\int_0^a Tr\mathrm{d}r \,/\int_0^a Pr\mathrm{d}r \;\;, \tag{5}$$

so that the total plasma energy and pedestal energies are given by

$$W_{\mathrm{Tot}} = 4\pi^2 RW \quad ; \quad W_{\mathrm{Ped}} = 3\pi^2 a^2 RnT_a \;, \tag{6}$$

respectively.

We normalise T to T_a, the edge temperature at $r = a$, introducing

$$\tau = \frac{T}{T_a},\; \rho = \frac{r}{a}, \qquad \lambda = \frac{Pr_0^2}{n\chi_0 T_a} \equiv \lambda_H\left(1 - \frac{P_{\mathrm{Rad}}}{P_{\mathrm{H}}}\right), \tag{7}$$

so that eqn. (1) becomes

$$\frac{1}{\rho}\frac{\mathrm{d}}{\mathrm{d}\rho}\left(\rho\frac{\mathrm{d}\tau}{\mathrm{d}\rho}\right) = -\frac{\lambda}{\rho_0^2} \tag{8}$$

where $\varrho_0 = r_0/a$. Condition (3) implies

$$\frac{1}{\tau}\frac{\mathrm{d}\tau}{\mathrm{d}\rho} = -\hat{c} \quad , \qquad \hat{c} = \frac{ca}{R} \tag{9}$$

and

$$W_{\text{Tot}} = \frac{W_{\text{Ped}}}{2} F(\rho_0, \lambda, \hat{c}) \; ; \; \tau_{\text{E}} = \frac{nT_a}{4P_{\text{H}} r_0^2} F(\rho_0, \lambda, \hat{c}) \; . \tag{10}$$

$F(\rho_0, \lambda, \hat{c})$ characterises the energy content as λ varies, but can also be used to yield the effects of varying the fraction of radiated power, $\gamma = P_{\text{Rad}}/P_{\text{H}}$, since the effect of radiative losses appears through the definition for λ in eqn. (7):

$$\lambda = \lambda_{\text{H}}(1-\gamma) \, , \qquad \lambda_{\text{H}} = \frac{P_{\text{H}} r_0^2}{n\chi_0 T_a} \; . \tag{11}$$

Thus, a change in the function $F(\rho_0, \lambda, \hat{c})$ as λ reduces can be interpreted as representing the effect of increasing radiative losses on τ_{E}. Interestingly, the effective stiffness parameter, $\hat{c}$, depends on aspect ratio, *R/a*, discriminating between conventional aspect ratio devices and spherical tokamaks (STs).

3. Solutions for Peaked Heating Profiles

To understand the significance of the various scenarios for the heating profile we consider the condition on λ for the onset of stiffness. Before the onset of stiffness, the solution of the transport equation for the temperature profile is:

$$\tau = \tau_0 - \frac{\lambda}{4} \frac{\rho^2}{\rho_0^2}, \quad 0 < \rho < \rho_0 \tag{12}$$

and

$$\tau = 1 - \frac{\lambda}{2} \ln\rho, \;\; \rho_0 < \rho < 1 \; . \tag{13}$$

Matching results (12) and (13) at $\rho = \varrho_0$, we obtain

$$\tau_0 = \frac{\lambda}{4} + 1 - \frac{\lambda}{2} \ln\rho_0 \; . \tag{14}$$

The onset condition for stiffness is given by eqn. (9). Substituting for τ from eqns. (12) and (13) and solving for λ, we find

$$\lambda_{\text{c}} = \frac{2\hat{c}\rho_0^2}{\left[\rho + \frac{\hat{c}\rho^2}{2} - \hat{c}\rho_0^2\left(\frac{1}{2} - \ln\rho_0\right)\right]}, \quad 0 < \rho < \rho_0 \tag{15}$$

and

$$\lambda_{\text{c}} = \frac{2\hat{c}\rho}{(1 + \hat{c}\rho\ln\rho)} \; , \quad \rho_0 < \rho < 1 \; , \tag{16}$$

where λ_c is the critical value of λ for the onset of a stiff temperature profile at a radius ρ. These match at $\rho = \rho_0$ of course. While solution (16) first increases inwards, it has a maximum at $\rho = 1/\hat{c} < 1$, so its lowest value may lie inside $\rho = 1/\hat{c}$ if $\hat{c}\rho_0 < 1$. In fact, this situation gives rise to two possibilities, as will be discussed later. Both solutions (15) and (16) suggest infinite values of λ_c may be needed at some radii, but since parts of the profile will already be stiff by the time these values are approached, these are spurious: these two solutions only pertain to the first onset of stiffness and are only used below to understand where this first happens. Following the onset of stiffness, the right-hand sides of eqns. (15) and (16) are modified as described below. As we will see, two main cases emerge: case (i) for $\hat{c}\rho_0 > 1$ and case (ii) for $\hat{c}\rho_0 < 1$, with the second dividing into two subcases, (ii a) and (ii b), depending on where ρ_0 lies relative to another critical radius, ρ_{2c}, to be defined below. These three scenarios are shown in Figs. 1 (a) to (c), where the values of λ_c for the onset of the critical gradients are plotted against ρ.

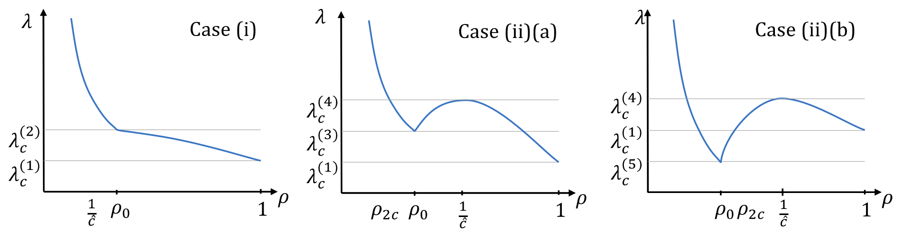

FIGURE 1. Schematic diagrams showing the critical values of λ for the onset of stiff temperature profiles, as a function of plasma radius, ρ. (a) case (i); (b) case (ii); subcase a; and (c) case (ii) subcase b. The dashed horizontal lines separate the different zones of λ used in calculating F, as defined in the text, leading to differing numbers of intersections as λ increases.

(i) Case $\hat{c}\rho_0 > 1$

In this case stiffness moves steadily inwards from $\rho = 1$ where the critical gradient condition is first satisfied. This occurs when

$$\lambda = \lambda_c^{(1)} = 2\hat{c} \quad . \tag{17}$$

Thereafter the onset of the stiff profile

$$\tau = e^{\hat{c}(1-\rho)} \tag{18}$$

occurs at $\rho = \rho_1(\hat{c}, \lambda, \rho_0)$, where ρ_1 is given by

$$\lambda = 2\hat{c}\rho_1 e^{\hat{c}(1-\rho_1)} \tag{19}$$

and steadily migrates inward as λ increases, since the condition (18) implies

$$2\hat{c}(1-\hat{c}\varrho_1)\frac{\mathrm{d}\rho_1}{\mathrm{d}\lambda}=1, \tag{20}$$

so that $\mathrm{d}\rho_1/\mathrm{d}\lambda<0$ for case (i).

First considering the situation $\rho_0<\rho_1$, we match the solutions (13) and (18) at $\rho=\rho_1$ and (12) and (13), which is now modified by the stiff region, at $\rho=\rho_0$ to obtain

$$\tau=e^{\hat{c}(1-\rho_1)}+\frac{\lambda}{2}\left[\ln\left(\frac{\rho_1}{\rho_0}\right)+\frac{1}{2}\right]-\frac{\lambda}{4}\frac{\rho^2}{\rho_0^2},\quad \rho<\rho_0, \tag{21}$$

$$\tau=\mathrm{e}^{\hat{c}(1-\rho_1)}+\frac{\lambda}{2}\ln\left(\frac{\rho_1}{\rho}\right),\quad \rho_0<\rho<\rho_1 \tag{22}$$

and

$$\tau=\mathrm{e}^{\hat{c}(1-\rho)};\quad \rho_1<\rho<1. \tag{23}$$

(In general, when we mention matching to the transport solution, eqn. (13), it may be modified by the imposition of a new outer boundary condition due to the intervention of a stiff region.)

Next, we consider the case $\rho_1<\rho_0$ when matching to eqn. (12) to eqn. (18) yields a modified equation for ρ_1:

$$\lambda\left(\frac{\rho_1}{\rho_0}\right)=2\hat{c}\rho_0\mathrm{e}^{\hat{c}(1-\rho_1)}\quad , \tag{24}$$

together with

$$\tau=\mathrm{e}^{\hat{c}(1-\rho_1)}+\frac{\lambda}{4\rho_0^2}(\rho_1^2-\rho^2),\quad 0<\rho<\rho_1 \tag{25}$$

and

$$\tau=\mathrm{e}^{\hat{c}(1-\rho)},\quad \rho_1<\rho<1. \tag{26}$$

Equation (25) implies

$$-2\hat{c}\rho_1(1+\hat{c}\rho_1)\frac{\mathrm{d}\rho_1}{\mathrm{d}\lambda}=\frac{\rho_1^2}{\rho_0^2}\quad , \tag{27}$$

again ensuring $\mathrm{d}\rho_1/\mathrm{d}\lambda<0$, so that ρ_1 continues to migrate inwards.

The expressions (12 - 14), (21 - 23), (25) and (26) for τ can be used to calculate the function $F(\lambda,\hat{c},\rho_0)$ characterising the plasma energy. It takes different forms, dependent on λ. It is useful to define several integrals that arise in calculating the various contributions to the plasma energy:

$$F(\rho_a,\rho_b) = 2\int_{\rho_a}^{\rho_b} \rho\tau \mathrm{d}\rho \quad . \tag{28}$$

Thus, we have $F_j(\rho_a,\rho_b)$, where

$$F_0(\rho_a,\rho_b) = 2\int_{\rho_a}^{\rho_b} \rho \mathrm{d}\rho;\ F_1(\rho_a,\rho_b) = 2\int_{\rho_a}^{\rho_b} \rho\ln\rho \mathrm{d}\rho\,;$$

$$F_2(\rho_a,\rho_b) = 2\int_{\rho_a}^{\rho_b} \frac{\rho^3}{\rho_0^2}\mathrm{d}\rho\,; \qquad F_3(\rho_a,\rho_b) = 2\int_{\rho_a}^{\rho_b} \mathrm{e}^{\hat{c}(1-\rho)}\rho \mathrm{d}\rho. \tag{29}$$

Specifically,

$$F_0(\rho_a,\rho_b) = (\rho_b^2-\rho_a^2),$$

$$F_1(\rho_a,\rho_b) = \left(\rho_b^2\left(\ln\rho_b - \frac{1}{2}\right) - \rho_a^2\left(\ln\rho_a - \frac{1}{2}\right)\right),$$

$$F_2(\rho_a,\rho_b) = \frac{1}{2\varrho_0^2}(\rho_b^4-\rho_a^4)\,,$$

$$F_3(\rho_a,\rho_b) = \frac{2}{\hat{c}^2}\left[(1+\hat{c}\rho_a)\mathrm{e}^{\hat{c}\,(1-\rho_a)} - (1+\hat{c}\rho_b)\mathrm{e}^{\hat{c}\,(1-\rho_b)}\right]. \tag{30}$$

For $\lambda < \lambda_{\mathrm{c}}^{(1)} = 2\hat{c}$,

$$F = \left(1+\frac{\lambda}{4}-\frac{\lambda}{2}\ln\rho_0\right)F_0(0,\rho_0) - \frac{\lambda}{4}F_2(0,\rho_0) + F_0(\rho_0,1) - \frac{\lambda}{2}F_1(\rho_0,1)\,, \tag{31}$$

so that

$$F = \left(1+\frac{\lambda}{4}\right) - \frac{\lambda\rho_0^2}{8}. \tag{32}$$

For $\lambda_{\mathrm{c}}^{(1)} < \lambda < \lambda_{\mathrm{c}}^{(2)} = 2\hat{c}\rho_0\mathrm{e}^{\hat{c}(1-\rho_0)}$,

$$F = \left\{\mathrm{e}^{\hat{c}(1-\rho_1)} + \frac{\lambda}{2}\left[\ln\left(\frac{\rho_1}{\rho_0}\right)+\frac{1}{2}\right]\right\}F_0(0,\rho_0) - \frac{\lambda}{4}F_2(0,\rho_0) + \left\{\mathrm{e}^{\hat{c}(1-\rho_1)} + \frac{\lambda}{2}\ln(\rho_1)\right\}F_0(\rho_0,\rho_1) - \frac{\lambda}{2}F_1(\rho_0,\rho_1) + F_3(\rho_1,1)\,, \tag{33}$$

so that

$$F = 2\mathrm{e}^{\hat{c}(1-\rho_1)}\left[\frac{(1+\hat{c}\rho_1)}{\hat{c}^2}+\frac{\rho_1^2}{2}\right] - \frac{2(1+\hat{c})}{\hat{c}^2} + \frac{\lambda}{4}\left[\rho_1^2-\frac{\rho_0^2}{2}\right] \quad , \tag{34}$$

where ρ_1 is given by

$$\lambda = 2\hat{c}\rho_1\mathrm{e}^{\hat{c}(1-\rho_1)} \quad . \tag{35}$$

For $\lambda_c^{(2)} < \lambda$,

$$F = \left[e^{\hat{c}(1-\rho_1)} + \frac{\lambda\rho_1^2}{4\rho_0^2}\right] F_0(0,\rho_1) - \frac{\lambda}{4} F_2(0,\rho_1) + F_3(\rho_1, 1), \tag{36}$$

leading to

$$F = 2e^{\hat{c}(1-\rho_1)}\left[\frac{(1+\hat{c}\rho_1)}{\hat{c}^2} + \frac{\rho_1^2}{2}\right] - \frac{2(1+\hat{c})}{\hat{c}^2} + \frac{\lambda}{8}\frac{\rho_1^4}{\rho_0^2} \quad , \tag{37}$$

where ρ_1 is now given by

$$\lambda\left(\frac{\rho_1}{\rho_0}\right) = 2\hat{c}\rho_0 e^{\hat{c}(1-\rho_1)}. \tag{38}$$

Equation (24) implies

$$-2\hat{c}\varrho\rho_1(1+\hat{c}\rho_1)\frac{d\rho_1}{d\lambda} = \frac{\rho_1^2}{\rho_0^2} \quad , \tag{39}$$

again ensuring $d\rho_1/d\lambda < 0$, so that ρ_1 continues to migrate inwards.

(ii) Case $\hat{c}\rho_0 < 1$

In this case the critical value of λ for the onset of stiffness, given by eqn. (16), is satisfied at two values of ρ , say ρ_1 and ρ_2, provided $\rho_0 < \rho_2$, as eqn. (16) only applies then. Since the critical value of λ corresponding to ρ_1 is $2\hat{c}$, eqn. (16) implies that the corresponding value of ρ_2 , which we denote by ρ_{2c}, is given by

$$\rho_{2c}(\hat{c}) = (1 + \hat{c}\rho_{2c}\ln\rho_{2c}). \tag{40}$$

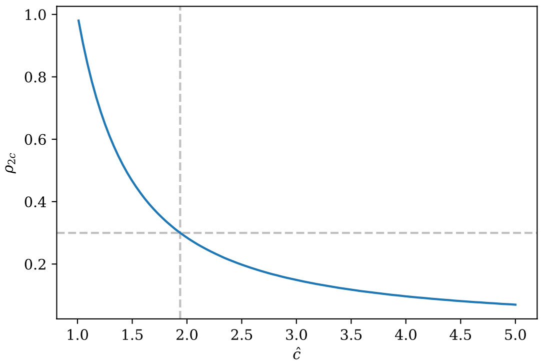

FIGURE 2. The variation of ρ_{2c} with $\hat{c}$; it is compared with $\rho_0 = 0.3$ as an example.

Figure 2 shows ρ_{2c} as a function of $\hat{c}$ which can be compared with ρ_0 ($\rho_0 = 0.3$ is shown for comparison, as an example).

Thus, if $\rho_0 > \rho_{2c}$ stiffness first sets in at $\rho = 1$, while if $\rho_0 < \rho_{2c}$, it begins at an interior point. We thus define two sub-cases - (a): $\rho_0 > \rho_{2c}$ and (b): $\rho_0 < \rho_{2c}$.

Sub-case (a): $\rho_0 > \rho_{2c}$

As before, stiffness onsets at $\rho = 1$ when $\lambda = 2\hat{c} = \lambda_c^{(1)}$ and solution (18) for τ holds until ϱ_1 satisfies condition (19) for a given λ. For smaller values of ρ, τ is given by eqn. (22). However, solution (22) will satisfy the condition for the onset of stiffness at a second point, ρ_2 , given by

$$\lambda_c = \frac{2\hat{c}\rho_2\, e^{\hat{c}(1-\rho_1)}}{(1+\hat{c}\rho_2 \ln(\rho_2/\rho_1))} \quad , \tag{41}$$

provided $\rho_2 > \rho_0$, of course. (Equation (41) is the modified form of eqn. (16), mentioned earlier.) Equation (19) for ρ_1 then implies a relationship between ρ_1 and ρ_2:

$$\rho_2 = \varrho_1 \left(1 + \hat{c}\rho_2 \ln\left(\frac{\rho_2}{\rho_1}\right)\right) \ . \tag{42}$$

The expression (41) still has a maximum at $\rho = 1/\hat{c}$ and differentiation of relation (42) shows that, because $\hat{c}\rho_2 < 1$ and $\hat{c}\rho_1 > 1$, ρ_2 moves outwards towards $\rho = 1/\hat{c}$, as ρ_1 moves inwards towards the same point. The condition $\rho_2 = \rho_0$ defines $\bar{\rho}_1$, a corresponding value for ρ_1, from eqn. (42) and a critical value $\lambda_c^{(3)}$ for λ from the relationship (30):

$$\lambda_c^{(3)} = 2\hat{c}\bar{\rho}_1 e^{\hat{c}(1-\bar{\rho}_1)} , \tag{43}$$

where

$$\rho_0 = \bar{\rho}_1 \left(1 + \hat{c}\rho_0 \ln\left(\frac{\rho_0}{\bar{\varrho}_1}\right)\right) . \tag{44}$$

Thus as λ increases there is a first onset of stiffness at $\rho = 1$ when $\lambda = 2\hat{c} = \lambda_c^{(1)}$; when $\lambda > \lambda_c^{(3)}$ there is a stiff region between ρ_0 and ρ_2 , with the region $\rho_2 < \rho < \rho_1$ being governed by the transport solution (22). The stiff region between ρ_0 and ρ_2 extends into the region $\rho < \rho_0$ as far as a radius ρ_3 , with ρ_3 relabelling ρ_1 in condition (19).

This situation prevails until λ reaches the value at the maximum of eqn. (41) at $\rho_1 = 1/\hat{c}$, namely

$$\lambda_{\mathrm{c}}^{(4)} = 2\mathrm{e}^{\hat{c}-1}. \tag{45}$$

Finally, for $\lambda > \lambda_{\mathrm{c}}^{(4)}$, the profile is stiff as far in as $\rho = \rho_3$.

Consequently, for $\lambda < 2\hat{c} = \lambda_{\mathrm{c}}^{(1)}$, τ is given by eqns. (12) - (13) again.

For $\lambda_{\mathrm{c}}^{(3)} < \lambda < \lambda_{\mathrm{c}}^{(1)}$, we again have τ given by eqns. (21) – (23).

For $\lambda_{\mathrm{c}}^{(3)} < \lambda < \lambda_{\mathrm{c}}^{(4)}$,

$$\tau = \mathrm{e}^{\hat{c}(1-\varrho)};\ \rho_1 < \rho < 1 \ , \tag{46}$$

as in eqn. (18), but solution (22) now has a restricted range:

$$\tau = \mathrm{e}^{\hat{c}(1-\rho_1)} + \frac{\lambda}{2}\ln\left(\frac{\rho_1}{\rho}\right);\ \rho_2 < \rho < \rho_1 \ . \tag{47}$$

Matching a stiff solution at $\varrho = \varrho_2$ to solution (47) we have

$$\tau = \mathrm{e}^{\hat{c}(1-\rho_1+\rho_2-\rho)} + \frac{\lambda}{2}\ln\left(\frac{\rho_1}{\rho_2}\right)\mathrm{e}^{\hat{c}(\rho_2-\rho)};\ \rho_3 < \rho < \rho_2 \ . \tag{48}$$

The radius ρ_3 is set by the onset of stiffness in the region $\rho < \rho_0$. Matching the stiff solution (48) to the transport solution defined by eqns. (12) – (13) leads to an equation for ρ_3:

$$\frac{\lambda\rho_3}{\rho_0} = 2\hat{c}\rho_0\left[\mathrm{e}^{\hat{c}(1-\rho_1+\rho_2-\rho_3)} + \frac{\lambda}{2}\ln\left(\frac{\rho_1}{\rho_2}\right)\mathrm{e}^{\hat{c}(\rho_2-\rho_3)}\right] \tag{49}$$

and an expression for τ:

$$\tau = e^{\hat{c}(1-\rho_1+\rho_2-\rho_3)} + \frac{\lambda}{2}\ln\left(\frac{\rho_1}{\rho_2}\right)\mathrm{e}^{\hat{c}(\rho_2-\rho_3)} + \frac{\lambda}{4}\frac{(\rho_3^2-\rho^2)}{\rho_0^2}, \rho < \rho_3. \tag{50}$$

Finally, for $\lambda > \lambda_{\mathrm{c}}^{(4)}$, the profile is stiff as far in as $\rho = \rho_3$, with ρ_3 relabelling ρ_1 in condition (19):

$$\frac{\lambda\rho_3}{\rho_0} = 2\hat{c}\rho_0\mathrm{e}^{\hat{c}(1-\rho_3)} \ , \tag{51}$$

so that

$$\tau = \mathrm{e}^{\hat{c}(1-\rho)},\quad \rho_3 < \rho < 1 \tag{52}$$

and

$$\tau = \mathrm{e}^{\hat{c}(1-\rho_3)} + \frac{\lambda}{4}\frac{(\rho_3^2-\rho^2)}{\rho_0^2},\ \rho < \rho_3. \tag{53}$$

It remains to calculate the corresponding function F.

For $\lambda < 2\hat{c} = \lambda_{\rm c}^{(1)}$ it is again given by expression (32) and for $\lambda_{\rm c}^{(3)} > \lambda > \lambda_{\rm c}^{(1)}$ by the result (34).

For $\lambda_{\rm c}^{(3)} < \lambda < \lambda_{\rm c}^{(4)}$, we have, using eqns. (46 - 48) and (50) for τ,

$$F = F_3(\rho_1, 1) + \left(\mathrm{e}^{\hat{c}(1-\rho_1)} + \frac{\lambda}{2}\ln(\rho_1)\right) F_0(\rho_2, \rho_1) - \frac{\lambda}{2} F_1(\rho_2, \rho_1) + \left[\mathrm{e}^{\hat{c}(\rho_2-\rho_1)} + \frac{\lambda}{2}\ln\left(\frac{\rho_1}{\rho_2}\right)\mathrm{e}^{\hat{c}(\rho_2-1)}\right] F_3(\rho_3, \rho_2) + \left[\mathrm{e}^{\hat{c}(1-\rho_1+\rho_2-\rho_3)} + \frac{\lambda}{2}\ln\left(\frac{\rho_1}{\rho_2}\right)\mathrm{e}^{\hat{c}(\rho_2-\rho_3)} + \frac{\lambda}{4}\frac{\rho_3^2}{\rho_0^2}\right] F_0(0, \rho_3) - \frac{\lambda}{4} F_2(0, \rho_3) \quad , \tag{54}$$

with $\lambda = 2\hat{c}\rho_1\mathrm{e}^{\hat{c}(1-\rho_1)}$, $\rho_2 = \varrho_1(1 + \hat{c}\rho_2\ln(\rho_2/\rho_1))$, and $\lambda\rho_3/\rho_0 = 2\hat{c}\rho_0\left[\mathrm{e}^{\hat{c}(1-\rho_1+\rho_2-\rho_3)} + \frac{\lambda}{2}\ln(\rho_1/\rho_2)\mathrm{e}^{\hat{c}(\rho_2-\rho_3)}\right]$,

which reduces to

$$F = 2\mathrm{e}^{\hat{c}(1-\rho_1+\rho_2-\rho_3)}\left[\frac{(1+\hat{c}\rho_3)}{\hat{c}^2} + \frac{\rho_3^2}{2}\right] + 2\mathrm{e}^{\hat{c}(1-\rho_1)}\left[\frac{\rho_1^2}{2} - \frac{\rho_2^2}{2} + \frac{(1+\hat{c}\rho_1)}{\hat{c}^2} - \frac{(1+\hat{c}\rho_2)}{\hat{c}^2}\right] - \frac{2(1+\hat{c})}{\hat{c}^2} + \frac{\lambda}{4}(\rho_1^2 - \rho_2^2) + \frac{\lambda\rho_3^4}{8\rho_0^2} + \lambda\ln\left(\frac{\rho_1}{\rho_2}\right)\left[\mathrm{e}^{\hat{c}(\rho_2-\rho_3)}\left(\frac{(1+\hat{c}\rho_3)}{\hat{c}^2} + \frac{\rho_3^2}{2}\right) - \frac{(1+\hat{c}\rho_2)}{\hat{c}^2} - \frac{\rho_2^2}{2}\right] . \tag{55}$$

Finally, for $\lambda > \lambda_{\rm c}^{(4)}$, using eqns. (52) and (53) for τ,

$$F = F_3(\rho_3, 1) + \left(\mathrm{e}^{\hat{c}(1-\rho_3)} + \frac{\lambda}{4}\frac{\rho_3^2}{\rho_0^2}\right) F_0(0, \rho_3) - \frac{\lambda}{4} F_2(0, \rho_3) \quad , \tag{56}$$

with ρ_3 now given by $\lambda\rho_3/\rho_0 = 2\hat{c}\rho_0\mathrm{e}^{\hat{c}(1-\rho_3)}$,

so that

$$F = 2\mathrm{e}^{\hat{c}(1-\rho_3)}\left[\frac{(1+\hat{c}\rho_3)}{\hat{c}^2} + \frac{\rho_3^2}{2}\right] - \frac{2(1+\hat{c})}{\hat{c}^2} + \frac{\lambda\rho_3^4}{8\rho_0^2} . \tag{57}$$

Sub-case (b): $\rho_0 < \rho_{2c}$

In this case the onset of stiffness occurs at the internal point ρ_0 and as λ increases beyond this critical value, a stiff region, $\rho_2 > \rho > \rho_3$, opens out around ρ_0 before the onset of stiffness at $\rho_1 = 1$. Further increases in λ lead to a similar evolution to that in sub-case (a); the transport-controlled region between ρ_2 and ρ_1 shrinking and eventually disappearing, with a stiff profile covering the entire region $1 > \rho > \rho_3$.

According to eqn. (16) the onset of stiffness at $\rho = \rho_0$ occurs when

$$\lambda = \lambda_{\mathrm{c}}^{(5)} = \frac{2\hat{c}\rho_0}{(1+\hat{c}\rho_0 \ln\rho_0)} \quad . \tag{58}$$

As λ increases beyond $\lambda_c^{(5)}$, the outer limit of stiffness, ρ_2, is determined by matching a stiff solution to the transport-controlled solution (13),

$$\tau = 1 - \frac{\lambda}{2}\ln\rho, \;\; \rho_2 < \rho < 1 \,, \tag{59}$$

yielding the equation:

$$\lambda = \frac{2\hat{c}\rho_2}{(1+\hat{c}\rho_2 \ln\rho_2)} \quad . \tag{60}$$

The form of the stiff solution within $\rho_2 > \rho > \rho_3$ is obtained by matching it to the solution (59) at $\rho = \rho_2$:

$$\tau = \left(1 - \frac{\lambda}{2}\ln(\rho_2)\right)\mathrm{e}^{\hat{c}(\varrho_2 - \rho)}, \quad \rho_2 > \rho > \rho_3 \quad . \tag{61}$$

This can then be matched to solution (12) at $\rho = \rho_3$ to determine τ_0 and hence the form of τ, which then provides an equation for ρ_3 by imposing the stiffness condition. We find

$$\tau = \mathrm{e}^{\hat{c}(\rho_2 - \rho_3)}\left(1 - \frac{\lambda}{2}\ln(\rho_2)\right) + \frac{\lambda}{4}\frac{(\rho_3^2 - \rho^2)}{\rho_0^2} \,, \quad \rho < \rho_3 \tag{62}$$

and that ρ_3 is determined by:

$$\frac{\lambda\rho_3}{\rho_0} = 2\hat{c}\rho_0 \mathrm{e}^{\hat{c}(\rho_2 - \rho_3)}\left(1 - \frac{\lambda}{2}\ln(\rho_2)\right). \tag{63}$$

When $\lambda = \lambda_{\mathrm{c}}^{(1)}$ there is the onset of stiffness at $\rho = 1$, so that, as in eqns. (46) and (47),

$$\tau = \mathrm{e}^{\hat{c}(1-\rho)};\; \rho_1 < \rho < 1 \tag{64}$$

and

$$\tau = \mathrm{e}^{\hat{c}(1-\rho_1)} + \frac{\lambda}{2}\ln\left(\frac{\rho_1}{\rho}\right);\; \rho_2 < \rho < \rho_1 \;. \tag{65}$$

This modifies eqn. (60) for $\varrho_2(\lambda)$, which becomes

$$\lambda = \frac{2\hat{c}\rho_2\, \mathrm{e}^{\hat{c}(1-\rho_1)}}{(1+\hat{c}\rho_2 \ln\,(\rho_2/\rho_1)} \quad . \tag{66}$$

The stiff solution (61) is also modified:

$$\tau = \left[\mathrm{e}^{\hat{c}(1-\rho_1)} - \frac{\lambda}{2}\ln\left(\frac{\rho_2}{\rho_1}\right)\right]\mathrm{e}^{\hat{c}(\rho_2 - \rho)}, \quad \rho_3 < \rho < \rho_2, \tag{67}$$

as are the results (62) and (63):

$$\tau = \mathrm{e}^{\hat{c}(1-\rho_1+\rho_2-\rho_3)} - \frac{\lambda}{2}\ln\left(\frac{\rho_2}{\rho_1}\right)\mathrm{e}^{\hat{c}(\rho_2-\rho_3)} + \frac{\lambda}{4}\frac{(\rho_3^2-\rho^2)}{\rho_0^2}\ , \quad \rho < \rho_3 \tag{68}$$

and

$$\frac{\lambda\rho_3}{\rho_0} = 2\hat{c}\rho_0\left[\mathrm{e}^{\hat{c}(1-\rho_1+\rho_2-\rho_3)} - \frac{\lambda}{2}\ln\left(\frac{\rho_2}{\rho_1}\right)\mathrm{e}^{\hat{c}(\rho_2-\rho_3)}\right]\ . \tag{69}$$

Finally, when $\lambda = \lambda_{\mathrm{c}}^{(4)}$, the stiff region stretches inwards as far as ρ_3:

$$\tau = \mathrm{e}^{\hat{c}(1-\rho)}, \qquad \rho_3 < \rho < 1\ , \tag{70}$$

with ρ_3 now given by eqn. (63).

Again matching eqn. (70) to solution (12) determines τ_0 and hence τ for the region $\rho < \rho_3$:

$$\tau = \mathrm{e}^{\hat{c}(1-\rho_3)} + \frac{\lambda}{4}\frac{(\rho_3^2-\rho^2)}{\rho_0^2}\ , \quad \rho < \rho_3\ . \tag{71}$$

It remains to calculate the corresponding functions F.

For $\lambda < \lambda_{\mathrm{c}}^{(5)}$, result (32) still holds.

For $\lambda_{\mathrm{c}}^{(1)} > \lambda > \lambda_{\mathrm{c}}^{(5)}$ we use eqns. (59), (61) and (62) to obtain

$$F = F_0(\rho_2,1) - \frac{\lambda}{2}F_1(\rho_2,1) + \mathrm{e}^{-\hat{c}(1-\rho_2)}\left(1-\frac{\lambda}{2}\ln(\rho_2)\right)F_3(\rho_3,\rho_2) + \left[\mathrm{e}^{\hat{c}(\rho_2-\rho_3)}\left(1-\frac{\lambda}{2}\ln(\rho_2)\right) + \frac{\lambda}{4}\frac{\rho_3^2}{\rho_0^2}\right]F_0(0,\rho_3) - \frac{\lambda}{4}F_2(0,\rho_3), \tag{72}$$

with $\lambda = 2\hat{c}\rho_2/(1+\hat{c}\rho_2\ln\rho_2)$ and $\lambda\rho_3/\rho_0 = 2\hat{c}\rho_0\mathrm{e}^{\hat{c}(\rho_2-\rho_3)}\big(1-(\lambda/2)\ln(\rho_2)\big)$,

so that

$$F = \left(1+\frac{\lambda}{4}\right)(1-\rho_2^2) + \frac{\lambda\rho_3^4}{8\rho_0^2} + 2\left[\mathrm{e}^{\hat{c}(\rho_2-\rho_3)}\left(\frac{(1+\hat{c}\rho_3)}{\hat{c}^2}+\frac{\rho_3^2}{2}\right) - \frac{(1+\hat{c}\rho_2)}{\hat{c}^2}\right] - \lambda\ln(\rho_2)\left[\mathrm{e}^{\hat{c}(\rho_2-\rho_3)}\left(\frac{(1+\hat{c}\rho_3)}{\hat{c}^2}+\frac{\rho_3^2}{2}\right) - \left(\frac{(1+\hat{c}\rho_2)}{\hat{c}^2}+\frac{\rho_2^2}{2}\right)\right]\ . \tag{73}$$

For $\lambda_{\mathrm{c}}^{(4)} > \lambda > \lambda_{\mathrm{c}}^{(1)}$ we have, taking account of results (64), (65), (67) and (68),

$$F = F_3(\rho_1,1) + \left[\mathrm{e}^{\hat{c}(1-\rho_1)} + \frac{\lambda}{2}\ln(\rho_1)\right]F_0(\rho_2,\rho_1) - \frac{\lambda}{2}F_1(\rho_2,\rho_1) + \left[\mathrm{e}^{\hat{c}(1-\varrho_1)} - \frac{\lambda}{2}\ln\left(\frac{\varrho_2}{\varrho_1}\right)\right]\mathrm{e}^{-\hat{c}(1-\varrho_2)}F_3(\varrho_3,\varrho_2)\ +$$

$$\left[\mathrm{e}^{\hat{c}(1-\rho_1+\rho_2-\rho_3)} - \frac{\lambda}{2}\ln\left(\frac{\rho_2}{\varrho_1}\right)\mathrm{e}^{\hat{c}(\rho_2-\rho_3)} + \frac{\lambda}{4}\frac{\rho_3^2}{\rho_0^2}\right]F_0(0,\rho_3) - \frac{\lambda}{4}F_2(0,\rho_3), \quad (74)$$

with $\lambda = 2\hat{c}\rho_1\mathrm{e}^{\hat{c}(1-\rho_1)}$, $\lambda = 2\hat{c}\rho_2/\big(1+\hat{c}\rho_2\ln(\rho_2/\rho_1)\big)$ and $\lambda\rho_3/\rho_0 = 2\hat{c}\rho_0\big[\mathrm{e}^{\hat{c}(1-\rho_1+\rho_2-\rho_3)} - (\lambda/2)\ln(\rho_2/\rho_1)\mathrm{e}^{\hat{c}(\rho_2-\rho_3)}\big]$,

which reduces to

$$F - \frac{2(1+\hat{c})}{\hat{c}^2} + \frac{\lambda\rho_3^4}{8\rho_0^2} + \frac{\lambda}{4}(\rho_1^2 - \rho_2^2) + 2\mathrm{e}^{\hat{c}(1-\rho_1+\rho_2-\rho_3)}\left[\frac{(1+\hat{c}\rho_3)}{\hat{c}^2} + \frac{\rho_3^2}{2}\right] + 2\mathrm{e}^{\hat{c}(1-\rho_1)}\left[\frac{(1+\hat{c}\rho_1)}{\hat{c}^2} + \frac{\rho_1^2}{2} - \frac{(1+\hat{c}\rho_2)}{\hat{c}^2} - \frac{\rho_2^2}{2}\right] - \lambda\ln\left(\frac{\rho_2}{\rho_1}\right)\left[\mathrm{e}^{\hat{c}(\rho_2-\rho_3)}\left(\frac{(1+\hat{c}\rho_3)}{\hat{c}^2} + \frac{\rho_3^2}{2}\right) - \left(\frac{(1+\hat{c}\rho_2)}{\hat{c}^2} + \frac{\rho_2^2}{2}\right)\right]. \quad (75)$$

Finally, for $\lambda > \lambda_{\mathrm{c}}^{(4)}$, using results (70) and (71), we obtain

$$F = F_3(\rho_3, 1) + \left[\mathrm{e}^{\hat{c}(1-\rho_3)} + \frac{\lambda}{4}\frac{\rho_3^2}{\rho_0^2}\right]F_0(0,\rho_3) - \frac{\lambda}{4}F_2(0,\rho_3), \quad (76)$$

with $\lambda\rho_3/\rho_0 = 2\hat{c}\rho_0\mathrm{e}^{\hat{c}(1-\rho_3)}$,

or

$$F = 2\mathrm{e}^{\hat{c}(1-\rho_3)}\left[\frac{(1+\hat{c}\rho_3)}{\hat{c}^2} + \frac{\rho_3^2}{2}\right] - \frac{2(1+\hat{c})}{\hat{c}^2} + \frac{\lambda\rho_3^4}{8\rho_0^2} \quad . \quad (77)$$

4. A Gyro-Bohm Model

A more realistic model for the basic diffusivity is gyro-Bohm, which has a temperature dependence $\chi \sim T^{3/2}$. With this form the transport equation (1) can still be readily integrated, but for the function $u = \tau^{5/2}$, rather than τ itself. The structure of the results for u are identical to those for τ if we make the replacements

$$\lambda \rightarrow \bar{\lambda} = 5\,\lambda/2; \quad \hat{c} \rightarrow \bar{c} = 5\,\hat{c}/2. \quad (78)$$

Here λ is now defined with $\chi_0 \rightarrow \chi_a = \chi(r=a)$. u satisfies the same stiffness condition as τ when expressed in terms of $\bar{c}$. However, the integrals involved in the normalised plasma energy function F must be expressed in terms of $\tau = u^{2/5}$, which is a complication. The fact that $\bar{c}$ is significantly greater than $\hat{c}$ means that physically sensible values for $\bar{c}$ correspond to $\bar{c}\rho_0 > 1$, i.e., generally we need only consider the results for case (i).

The expressions for u can be used to construct

$$F = 2\int_0^1 \varrho\, u^{2/5}(\rho)\mathrm{d}\rho \quad . \tag{79}$$

We define

$$F_1(u_0, \rho_a, b) = 2\int_0^{\rho_a} \varrho\,(u_0 - b\rho^2)^{2/5}\,\mathrm{d}\rho$$

$$= \frac{5}{7b}\left[u_0^{7/5} - (u_0 - b\varrho_a^2)^{7/5}\right], \tag{80}$$

$$F_2(\rho_a, \rho_b, u_1, d\,) = 2\int_{\rho_a}^{\rho_b} \varrho\,(u_1 - d\,\ln\rho)^{2/5}\mathrm{d}\rho \tag{81}$$

$$= \left(\frac{d}{2}\right)^{2/5} \mathrm{e}^{2u_1/d}\left[\Gamma\left(\frac{7}{5}, \frac{2u_1}{d} - \ln\rho_a^2\right) - \Gamma\left(\frac{7}{5}, \frac{2u_1}{d} - \ln\rho_b^2\right)\right] \tag{82}$$

and

$$F_3(\rho_a, \rho_b) = 2\int_{\rho_a}^{\rho_b} \mathrm{e}^{\hat{c}(1-\rho)}\rho\mathrm{d}\rho$$

$$= \frac{2}{\hat{c}^2}\left[(1+\hat{c}\rho_a)\mathrm{e}^{\hat{c}\,(1-\rho_a)} - (1+\hat{c}\rho_b)\mathrm{e}^{\hat{c}\,(1-\rho_b)}\right]. \tag{83}$$

For $\bar{\lambda} < \bar{\lambda}_\mathrm{c}^{(1)} = 2\bar{c}$:

$$F = F_1\left(1 + \frac{\bar{\lambda}}{4} - \frac{\bar{\lambda}}{2}\ln\varrho_0\,, \rho_0, \frac{\bar{\lambda}}{4\rho_0^2}\right) + F_2\left(\rho_0, 1, \frac{\bar{\lambda}}{2}\right)\ , \tag{84}$$

so that

$$F = \frac{20\rho_0^2}{7\bar{\lambda}}\left[\left(1 + \frac{\bar{\lambda}}{4} - \frac{\bar{\lambda}}{2}\ln\varrho_0\right)^{7/5} - \left(1 - \frac{\bar{\lambda}}{2}\ln\varrho_0\right)^{7/5}\right] + \left(\frac{\bar{\lambda}}{4}\right)^{2/5}\exp\left(\frac{4}{\bar{\lambda}}\right)\left[\Gamma\left(\frac{7}{5}, \frac{4}{\bar{\lambda}}\right) - \Gamma\left(\frac{7}{5}, \frac{4}{\bar{\lambda}} - 2\ln\varrho_0\right)\right]\ ; \tag{85}$$

for $\bar{\lambda}_\mathrm{c}^{(1)} < \bar{\lambda} < \bar{\lambda}_\mathrm{c}^{(2)}$:

$$F = F_3(\rho_1, 1) + F_2\left(\rho_0, \rho_{1,}, e^{\bar{c}(1-\rho_1)} + \frac{\bar{\lambda}}{2}\ln\varrho_1, \frac{\bar{\lambda}}{2}\right) + F_1\left(\mathrm{e}^{\bar{c}(1-\rho_1)} + \frac{\bar{\lambda}}{2}\left(\ln\left(\frac{\varrho_1}{\varrho_0}\right) + \frac{1}{2}\right), \rho_0, \frac{\bar{\lambda}}{4\rho_0^2}\right), \tag{86}$$

leading to

$$F =$$

$$\frac{20\rho_0^2}{7\bar{\lambda}}\left[\left(e^{\bar{c}(1-\rho_1)}+\frac{\bar{\lambda}}{2}\left(\ln\left(\frac{\varrho_1}{\varrho_0}\right)+\frac{1}{2}\right)\right)^{7/5}-\left(e^{\bar{c}(1-\rho_1)}+\frac{\bar{\lambda}}{2}\ln\left(\frac{\varrho_1}{\varrho_0}\right)\right)^{7/5}\right]+$$
$$\left(\frac{\bar{\lambda}}{4}\right)^{2/5}\rho_1^2\exp\left(\frac{2}{\bar{c}\varrho_1}\right)\left[\Gamma\left(\frac{7}{5},\frac{2}{\bar{c}\varrho_1}\right)-\Gamma\left(\frac{7}{5},\frac{2}{\bar{c}\varrho_1}+2\ln\left(\frac{\varrho_1}{\varrho_0}\right)\right)\right]+\;2\,e^{\hat{c}(1-\rho_1)}\frac{(1+\hat{c}\varrho_1)}{\hat{c}^2}-$$
$$\frac{2(1+\hat{c})}{\hat{c}^2}. \tag{87}$$

Here we recall $\hat{c}=2\bar{c}/5$ is to be used in the last term and where ρ_1 is given by

$$\bar{\lambda}=2\bar{c}\rho_1 e^{\bar{c}(1-\rho_1)}\,. \tag{88}$$

For $\bar{\lambda}>\bar{\lambda}_c^{(2)}$ we have:

$$F=F_3(\rho_1,1)+\;F_1\left(e^{\bar{c}(1-\rho_1)}+\frac{\bar{\lambda}\rho_1^2}{4\rho_0^2},\rho_1,\frac{\bar{\lambda}}{4\rho_0^2}\right)\;, \tag{89}$$

with the result

$$F=\frac{20\rho_0^2}{7\bar{\lambda}}\left[\left(e^{\bar{c}(1-\rho_1)}+\frac{\bar{\lambda}\rho_1^2}{4\rho_0^2}\right)^{7/5}-e^{(7\bar{c}/5)(1-\rho_1)}\right]+$$
$$2\,e^{\hat{c}(1-\rho_1)}\frac{(1+\hat{c}\varrho_1)}{\hat{c}^2}-\frac{2(1+\hat{c})}{\hat{c}^2}, \tag{90}$$

where ρ_1 is now given by

$$\bar{\lambda}\left(\frac{\rho_1}{\rho_0}\right)=2\bar{c}\rho_0 e^{\bar{c}(1-\rho_1)}\quad. \tag{91}$$

In the above, $\Gamma(a,b\,)=\int_b^\infty e^{-t}t^a\,dt$ is the Incomplete Gamma Function [Abramowitz, & Stegun, 1972].

This simple gyro-Bohm model suffers from having a thermal diffusivity that decreases radially outwards, whereas experiment suggests otherwise. To remedy this, we have modified the above analysis by including an additional, radially increasing, factor so that $\chi\sim(1+\alpha\varrho^2)\tau^{3/2}$, with $\alpha\sim 0(1)$, a constant. This analysis is described in the Appendix.

5. Confinement Results

The various equations for the radii $\rho_{1,2,3}(\hat{\lambda})$ are solved numerically using Python [Virtanen *et al.*, 2019] and Brent's method [Brent, 1973] for the root solver. For both transport models it is useful to plot the various functions $F(\lambda,\hat{c},\,\rho_0)$ (or $F(\bar{\lambda},\bar{c},\rho_0)$) , normalised to the 'fully-stiff' limit F_∞ attained as $\lambda\to\infty$, against

$\hat{\lambda} = \lambda/\lambda_{\mathrm{c}}$ (or $\hat{\lambda} = \bar{\lambda}/\bar{\lambda}_{\mathrm{c}}$), i.e., normalised to the relevant critical value, $\lambda_{\mathrm{c}} = 2\hat{c}$, or $\bar{\lambda}_{\mathrm{c}} = 2\bar{c}$.

The quantity F_∞ follows from taking the limit ρ_1 (or ρ_3, as appropriate) $\to 0$. This leads to

$$F_\infty = \frac{2\mathrm{e}^{\hat{c}}}{\hat{c}^2} - \frac{2(1+\hat{c})}{\hat{c}^2} \ , \qquad (92)$$

which is a rapidly increasing function of $\hat{c}$. The results for the functions F are shown in Fig. 3 for the constant χ model and in Fig. 4 for the gyro-Bohm one, covering a range of relevant values of $\hat{c}$ and ρ_0. For these we choose $\rho_0 = 0.33, 0.66$ and 1.0 , ranging from a more centrally localised heating profile to one that is constant in radius. Since we expect $c = 4 - 6$ and the inverse aspect ratio, a/R , to typically range from 0.3 for conventional tokamaks to 0.6 for STs, we select $\hat{c} = 1.375, 2.75$ and 4.125 as being representative. This corresponds to $\bar{c} = 3.438, 6.875$ and 10.313. For the constant χ model this involves all three cases: (i), (ii a) and (ii b), while for the gyro-Bohm model only case (i) is needed for such plausible values of c and ρ_0 (although central heating by ECRH might involve the other two cases).

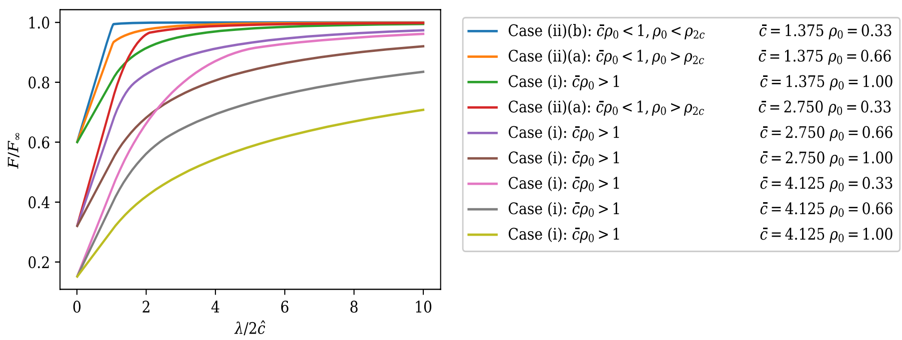

FIGURE 3. The variation of the function $F(\hat{\lambda}, \hat{c}, \rho_0)$, normalised to the asymptotic value, F_∞, characterising the plasma energy content, for the constant χ case, as a function of $\lambda/2\hat{c}$, representing the power dependence. $\rho_0 = 0.33, 0.66$ and 1.0 , ranging from more centrally localised heating to being constant in radius. $\hat{c} = 1.375, 2.75$ and 4.125 covering the range of critical gradients and aspect ratios from conventional tokamaks to spherical tokamaks

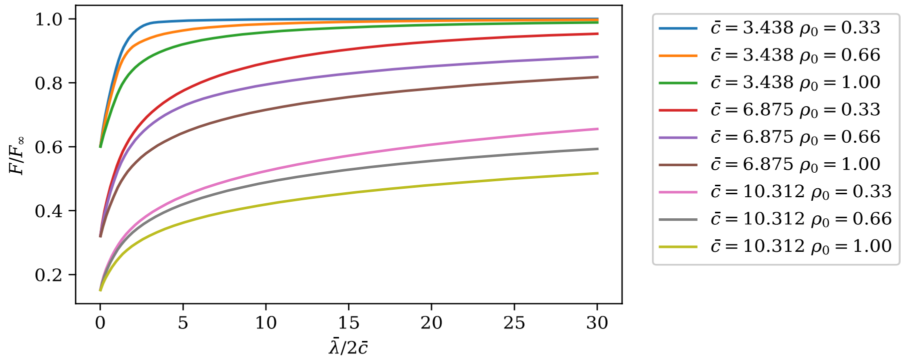

FIGURE 4. As for Figure 3, but for the gyro-Bohm model and in terms of $\bar{\lambda}$, with the corresponding values $\bar{c} = 3.438, 6.875$ and 10.313.

It is interesting to consider the special case of centrally localised heating, such as central electron cyclotron heating (ECRH), and investigate the limit of $\rho_0 \to 0$. Figure 5 shows the results for a sequence $\rho_0 = 0.01$ to 1.0 for the constant χ case and $\bar{c} = 1.375$.

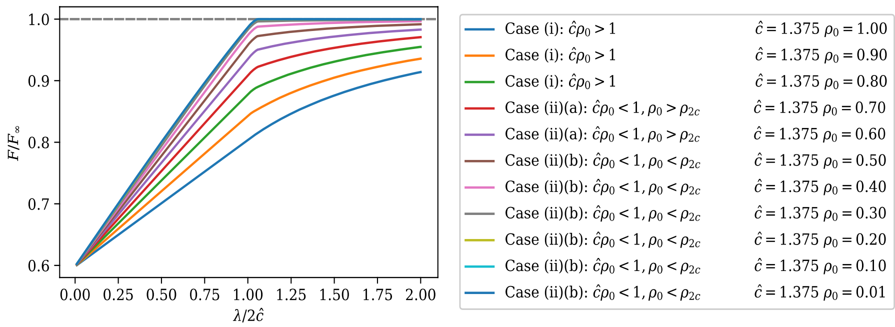

FIGURE 5. The convergence of $F(\hat{\lambda},, \hat{c}, \rho_0)$ to an asymptotic form for a sequence of values of ρ_0 approaching zero ($\rho_0 = 1.0 \to 0.01$ for the constant χ model with $\hat{c}$=1.375.

Commented [CJW1]:

Commented [CJW2R1]:

The impact of the modified gyro-Bohm model described in the Appendix on the function F is presented in Fig. 6 for $\rho_0 = 0.45$ and $\bar{c} = 6.875$, with the χ profile parameter taking the values $\alpha = 1$ and 2; the simple gyro-Bohm ($\alpha = 0$) and the constant χ (with the equivalent value of c) models are shown for comparison; this also allows a direct comparison of the two basic models .

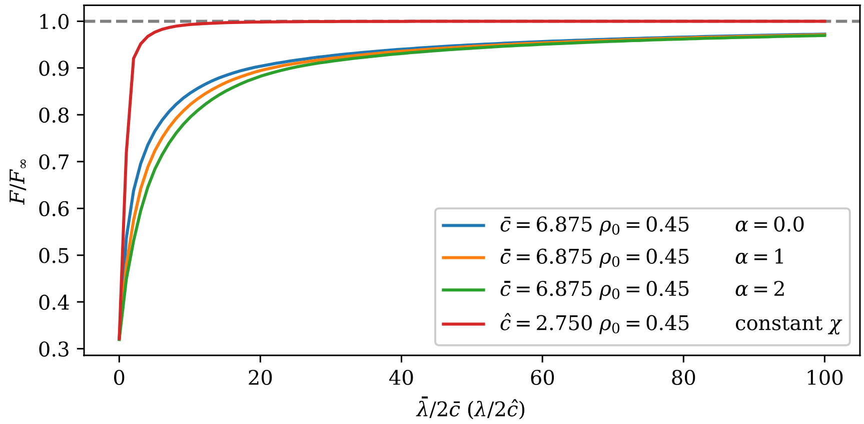

FIGURE 6. The effect of the χ profile parameter, α , of the improved gyro-Bohm model on the plasma energy content F for $\rho_0 = 0.45$ and $\bar{c} = 6.875$ with $\alpha = 1$, and 2. The simple gyro-Bohm case ($\alpha = 0$) and the constant χ case (for the equivalent value of c) are shown for comparison.

It is also illuminating to plot how ρ_1, ρ_2 and ρ_3 (where appropriate) migrate as λ increases, as shown in Fig.7(a) to 7(c) for some typical situations from cases (i), (ii a) and (ii b), respectively. These results indicate how the onset of stiffness develops as the net heating power increases and the stored plasma energy eventually saturates.

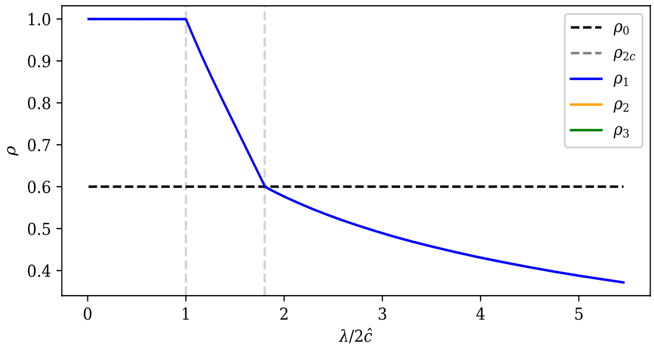

(a)

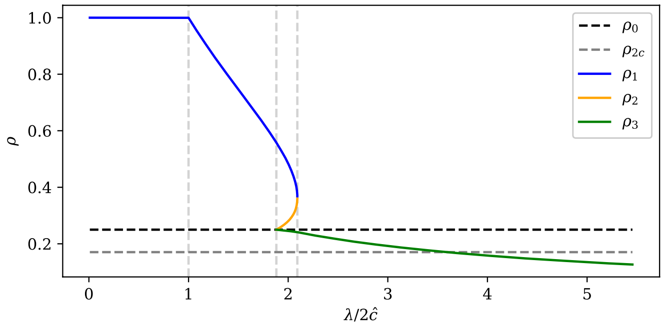

(b)

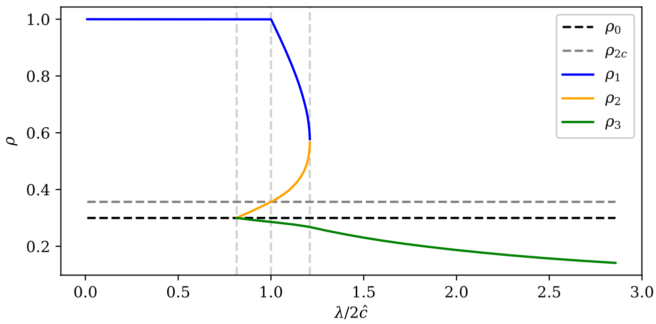

(c)

FIGURE 7. The evolution of $\rho_{1,2,3}(\hat{\lambda})$, the radii where the transitions to 'stiff' transport occur, as functions of the parameter $\hat{\lambda}$, representing the net heating power for the case of a constant thermal diffusivity. (a) $\rho_0 = 0.6$, $\hat{c} = 2.75$ represents case (i); (b) $\rho_0 = 0.25$, $\hat{c} = 2.75$ represents case (ii a); (c) $\rho_0 = 0.3$, $\hat{c} = 1.75$ represents case (ii b). ρ_{2c} is also shown.

To investigate the effect of radiative losses, we have calculated γ, the fractional reduction in λ, before F falls to 90% of its value, as a function of λ_H, corresponding to the additional heating power, P_{H} , as defined in eqn. (11). From eqn. (11) this value of γ can be interpreted as the fraction of impurity radiative power, P_{Rad}, to P_{H} (at constant P_{H}), that is allowed before the plasma energy is significantly reduced. This is plotted as a function of the normalised heating power, λ_{H}, in Fig. 8 for the gyro-Bohm model and representative values of $\bar{c}$ and ρ_0 ($\bar{c} = 3.438, 6.875$ and 10.132 with $\rho_0 = 0.33$ and 0.66).

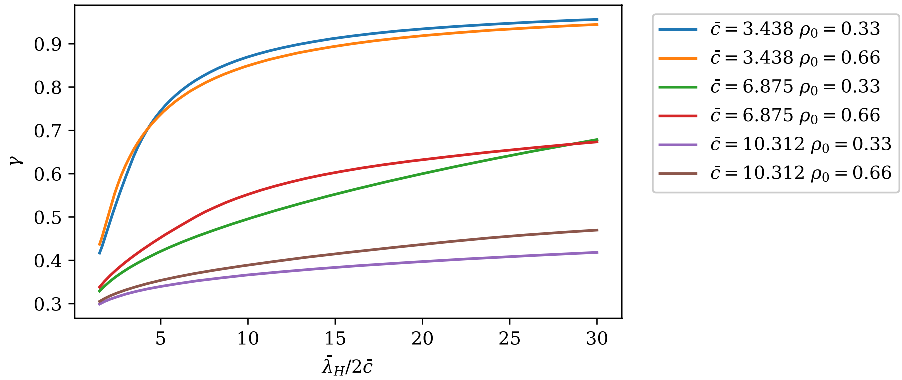

FIGURE 8. Allowed fraction of impurity radiative power, $\gamma = P_{\mathrm{Rad}}/P_{\mathrm{H}}$ before plasma energy content $F(\bar{\lambda}, \bar{c}, \rho_0)$ falls to 90% of its value as a function of $\bar{\lambda}_{\mathrm{H}}$, which corresponds to the heating power P_{H}, in the case of the gyro—Bohm model: $\rho_0 = 0.33$ and $\rho_0 = 0.66$ and , with $\bar{c} = 3.438, 6.875$ and 10.312.

These results indicate how the onset of stiffness develops as the net heating power increases and rate at which the stored plasma energy eventually saturates. Given the results for F, one could also infer how a normalised energy confinement time, $\hat{\tau}_{\mathrm{E,Rad}} = F(\lambda_{\mathrm{H}}(1-\gamma))/\lambda_{\mathrm{H}}$, (or just $F(\lambda_{\mathrm{H}}(1-\gamma))$) varies with λ_{H}, indicating the variation with net heating power, P, and with γ, showing the impact of impurity radiative losses. In the absence of radiative losses, so that $\gamma = 0$, this provides the basic normalised confinement time of course. However, here we only illustrate these effects for F itself, as shown in Fig. 9 for the gyro-Bohm transport model. The parameters chosen are $\bar{c} = 6.875$ and $\gamma = 0, 0.25, 0.5, 0.75$ and 0.9. Figure 9(a) is the case $\rho_0 = 0.66$ and Fig. 9(b) is $\rho_0 = 0.33$.

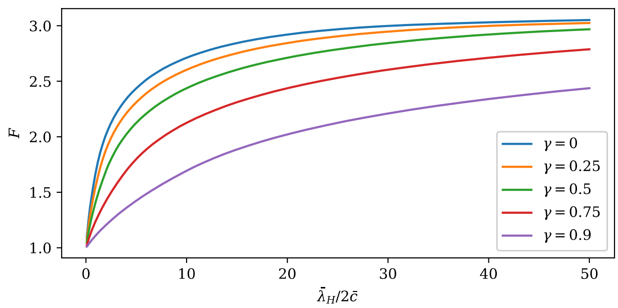

(a)

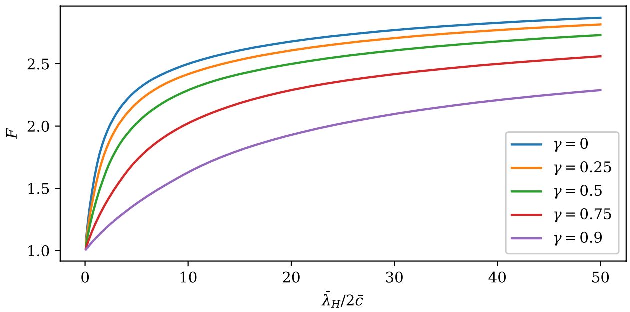

(b)

FIGURE 9. The effect of the impurity radiation fraction, $\gamma = P_{\mathrm{Rad}}/P_{\mathrm{H}}$, on the normalised energy content, $F(\bar{\lambda},\ \hat{c},\ \rho_0)$, with $\bar{\lambda}_H$, representing the heating power, P_{H}, and $\bar{\lambda} = \bar{\lambda}_{\mathrm{H}}(1-\gamma)$ representing the net heating allowing for impurity radiation, for the gyro-Bohm model with $\bar{c} = 6.875$ and $\gamma = 0,\ 0.2, 0.7$ and 0.9 for: (a) $\rho_0 = 0.33$ and (b) $\rho_0 = 0.66$.

6. Discussion and Conclusions

We have explored the effect of the onset of stiff temperature profiles on the plasma energy and energy confinement time as the net heating power, i.e., the difference between the applied heating power and the radiated power, increases and deduced how impurity radiation energy losses affect these results.

Two models for transport in any diffusive regions of the radial profile are considered: constant χ and gyro-Bohm, though a modified gyro-Bohm model which incorporates an additional radial profile factor is discussed in the Appendix; density is taken to be constant in radius, r. The net heating profile is 'box-like': constant for $r < r_0$ and zero beyond ($\varrho_0 = r_0/a = 0.33, 0.66, 1.0$ are taken as representative of more or less localised heating, respectively; for the case of central ECRH, it may be narrower of course, and is investigated separately. An H-mode edge pedestal temperature is taken, implying the heating power exceeds the L-H threshold value [ITER Expert Groups on Confinement and Confinement Modelling and Database, 1999, Doyle *et al*., 2007].

The condition for the onset of stiffness in the temperature profile is given by $\mathrm{dln}T/\mathrm{d}r = -c/R$, where typically $c \sim 4-6$. For the constant χ case this leads to a more useful normalised parameter, $\hat{c} = ca/R$; for the gyro-Bohm case this is replaced by $\bar{c} = 5ca/2R$. We can expect $\hat{c}$ to range from about 4/3 to 4 as a/R ranges from 2/3 for an ST to 1/3 for a more conventional tokamak;

correspondingly $\bar{c}$ ranges from about 10/3 to 10 for the gyro-Bohm model. Thus, we see STs are more resilient to stiff profiles.

We have considered how the plasma energy content varies as the heating power increases. We have defined a quantity F , the normalised plasma energy $W_{\text{Tot}} = 6\pi^2 R \int_0^a nT\, r\mathrm{d}r$, is relative to the pedestal energy, $W_{\text{Ped}} = 3\pi^2 n T_a R a^2$. The net heating power is parametrised by a quantity $\lambda = Pr_0^2/n\chi_0 T_a$(or $\bar{\lambda} = 5Pr_0^2/2n\chi_a T_a$ for the gyro-Bohm case). To interpret this more physically, we can re-write λ in terms of macroscopic quantities:

$$\lambda = \frac{3}{2}\frac{P_{\text{Tot}}\tau_{\text{Cond}}}{W_{\text{Ped}}}, \tag{93}$$

where P_{Tot} is the total net heating power (i. e., subtracting the total core radiation loss power) and $\tau_{\text{Cond}} = a^2/\chi_0$ (or a^2/χ_a for the gyro-Bohm model, where λ is replaced by $\bar{\lambda}$) is a confinement time corresponding to the thermal conduction mechanism.

We have explored how the function F responds to λ or $\bar{\lambda}$, as appropriate. In fact, to unify the results on a single plot, it is useful to consider $\hat{F} = F/F_\infty$, where $F_\infty = 2\mathrm{e}^{\hat{c}}/\hat{c}^2 - 2(1+\hat{c})/\hat{c}^2$, the value of F as $\lambda \to \infty$, as a function of $\hat{\lambda} = \lambda/2\hat{c}$; here the onset of stiffness at the plasma edge corresponds to $\hat{\lambda} = 1$. Note $\hat{\lambda} = \hat{\bar{\lambda}}$, at given values of P and c , where $\hat{\bar{\lambda}}$, is the corresponding quantity for the gyro-Bohm model, so the same scale can be used to compare the dependence on net heating power. The functions $\hat{F}$ are parametrised by ρ_0 and $\hat{c}$ (or $\bar{c}$, as is appropriate to the gyro-Bohm model). Furthermore, they take different forms for $\rho_0\hat{c} > 1$ (case (i)) or $\rho_0\hat{c} < 1$ (case (ii)). In fact, case (ii) sub-divides according as to whether $\rho_0 > \rho_{2\text{c}}(\hat{c})$ (sub-case (a)) or $\rho_0 < \rho_{2\text{c}}(\hat{c})$ (sub-case (b)], as explained in Fig.1; $\rho_{2\text{c}}(\hat{c})$ as a function of $\hat{c}$ is shown in Fig. 2. These cases correspond to different regions experiencing the onset of stiffness. In case (i) this begins at the plasma edge, in case (ii a), a second, interior, region subsequently emerges about ρ_0, whereas in case (ii b) it appears there first.

Results for $\hat{F}(\hat{c}, \rho_0, \hat{\lambda})$ are presented in Fig. 3 for the constant χ model and in Fig. 4 for the gyro-Bohm one (with appropriate re-definitions), for a physically reasonable range of the parameters. For the constant χ model this involves encountering all three cases, whereas for the gyro-Bohm model, only case (i) generally occurs. The result of allowing $\rho_0 \ll 1$, relevant to central ECRH, is shown in Fig. 5 for the constant χ model. Figure 6 shows the impact of the profile parameter α of the improved gyro-Bohm model, described in the Appendix, on the plasma energy content (note that this plot is for F/F_∞; F itself is proportional to a further factor $(1+\alpha)$). Increasing α (i.e. broadening the χ profile) makes the onset of stiffness progressively somewhat smoother than the simple gyro-Bohm case; the constant χ case (for the equivalent value of c) is sharper than the simple gyro-Bohm.

For the constant χ model, we show in Figs. 7(a) –(c) how the regions of stiffness (defined by up to three transition radii, ρ_1, ρ_2 and ρ_3) evolve in relation to ρ_0 for representative values of $\hat{c}$ and ρ_0 . Here ρ_1 represents the onset of a stiff region at the edge, while ρ_2 and ρ_3 define the limits of an interior stiff region. As the input power increases, i.e. λ increases, ρ_1 (or ρ_3 if appropriate) approaches zero asymptotically, so that $F \to F_\infty$, corresponding to a completely stiff profile. At low values of λ, before stiffness sets in, F takes the value unity, corresponding to the pedestal energy value, plus a linear dependence on λ for the constant χ model, before saturation eventually sets in, whereas for the gyro-Bohm model, it has a more complex dependence: linear in λ at first, increasing as $\lambda^{2/5}$ at larger λ, before saturation starts to occur. The stiffness onset, which occurs when $\lambda = 2\hat{c}$ (or $\bar{\lambda} = 2\bar{c}$) is also more gradual for the gyro-Bohm model. However, the variation of F with λ at the onset of stiffness becomes sharper as the heating becomes more localised. This is emphasized by allowing $\rho_0 \to 0$; Fig. 5 shows how the onset of stiffness becomes sharper and sharper, approaching an asymptotic limit.

One can also define a normalised energy confinement time, $\hat{\tau}_E$. Since

$$\tau_{\mathrm{E}} = \frac{W_{\mathrm{Ped}}}{P_{\mathrm{H,Tot}}} F(\lambda, \hat{c}, \varrho_0), \qquad (94)$$

eqn. (93) implies $\tau_{\mathrm{E}}(\lambda_{\mathrm{H}}) = 3\tau_{\mathrm{Cond}} F(\lambda, \hat{c}, \varrho_0)/2\lambda_{\mathrm{H}}$, where λ_{H} represents just the applied heating power. Thus, we define $\hat{\tau}_{\mathrm{E}}(\lambda_{\mathrm{H}}) = F(\lambda, \hat{c}, \varrho_0)/\lambda_{\mathrm{H}}$. If no impurity radiation is present, so that $\lambda = \lambda_{\mathrm{H}}$, $\hat{\tau}_{\mathrm{E}}$ represents the normal confinement time. It is in fact clearer to show just $F(\lambda, \hat{c}, \varrho_0)$; examples for the more realistic gyro-Bohm transport model are illustrated in Fig. 9, where the $\gamma = 0$ case ($\gamma = \lambda_{\mathrm{Rad}}/\lambda_{\mathrm{H}}$) shows the power dependence of the plasma energy content predicted by the modelling. For the energy confinement time itself, this case reflects the effects of diffusive transport at intermediate values of λ_{H} leading to a $\lambda_{\mathrm{H}}^{-3/5}$ power dependence, as anticipated for gyro-Bohm transport, with a sharper inverse power dependence as stiffness sets in, eventually varying like $1/\lambda_{\mathrm{H}}$.

The pedestal energy may also have some power dependence, but we only make some brief comments on that here. The pedestal energy appears to increase with higher values of β_{Pol}, the poloidal beta [Chapman *et al*., 2015, Connor *et al*., 2016]; indeed a scaling $T_{\mathrm{Ped}} \propto \beta_{\mathrm{Pol}}^{1/2}$ was found [Kirk *et al.*, 2009, Maggi *et al.*, 2016]. This would imply $W \propto F^2$, but the situation may be more complex.

The results for $F(\lambda, \hat{c}, \varrho_0)$ can also be used to infer the effect of P_{Rad} on the plasma energy and confinement. For a given level of heating power, P_{H}, introducing the impurity radiative losses can be expected to diminish the plasma energy. The amount can be quantified by seeing the effect on $F(\lambda, \hat{c}, \varrho_0)$ by reducing λ from λ_H (defined in terms of just P_{H}) to $\lambda_H(1 - P_{\mathrm{Rad}}/P_{\mathrm{H}})$ at constant λ_H. To be precise, we consider what reduction in λ from λ_H to λ_1, say, reduces $F(\lambda, \hat{c}, \varrho_0)$ by 90% as a function of $\lambda = \lambda_H$. The quantity $\delta\lambda = \lambda_{\mathrm{H}} - \lambda_1$ then represents $\lambda_{\mathrm{Rad}} = 3P_{\mathrm{Rad}}\tau_{\mathrm{Cond}}/2W_{\mathrm{Ped}}$, which determines the acceptable radiative power. Thus, this value of $\gamma = \lambda_{\mathrm{Rad}}/\lambda_{\mathrm{H}}$ at fixed λ_{H} is equivalent to the ratio of the acceptable level of radiative power relative to the heating, as a function of the latter. Figure 8 shows the variation of γ (at fixed $\bar{\lambda}_{\mathrm{H}}$) with $\bar{\lambda}_{\mathrm{H}}$ for the more realistic gyro-Bohm χ model. Clearly the results are rather insensitive to the width of the heating profile, but the radiative losses have a much greater effect on the plasma energy content at the larger values of $\hat{c}$. Figure 9 shows the equivalent impact of various levels of γ on the normalised plasma energy content, F, as a function of $\bar{\lambda}_{\mathrm{H}}$, showing how it moderates at the larger values of the heating power.

It is useful to fit these numerical results with a simpler analytic form that describes the effect of heating power on confinement. We construct a form for F that correctly recovers the linear form of the analytic, small $\bar{\lambda}$ expansion of eqn. (84), merges into the $\bar{\lambda}^{2/5}$ form, characteristic of gyro-Bohm transport, at somewhat larger values, before starting to saturate after the onset of critical gradients at $\bar{\lambda} = 2\bar{c}$. Eventually, it reaches the large $\bar{\lambda}$, asymptotic limit in eqn. (92). A reasonably good fit is

$$F_{fit} = 1 + \frac{\left\{\frac{\bar{c}\hat{\lambda}}{10}\left[1-2\{1-\rho_0^2\}\ln\rho_0^2\right]+b(F_\infty-1)\hat{\lambda}^{3/2}\right\}}{1+a\hat{\lambda}^{3/5}+b\hat{\lambda}^{3/2}}, \hat{\lambda} = \bar{\lambda}/2\bar{c}\,, \qquad (95)$$

where a and b are fitting parameters, dependent on $\bar{c}$ and ϱ_0.

Figure 10 shows a comparison of the fit (95) with the form of eqns. (85), (87) and (90) for the parameters of Fig. 4 for optimised values of a and b. For given values of $\bar{c}$, a and b depend on ϱ_0 as shown in Fig. 11, where the mean square errors characterising the ‘goodness of fit’ are also shown. Thus, the fit (95) for the plasma energy content includes a dependence on the heating profile. The dependence on the critical gradient parameter, $\bar{c}$, is complicated, but for a given stiff transport mode this value is well defined.

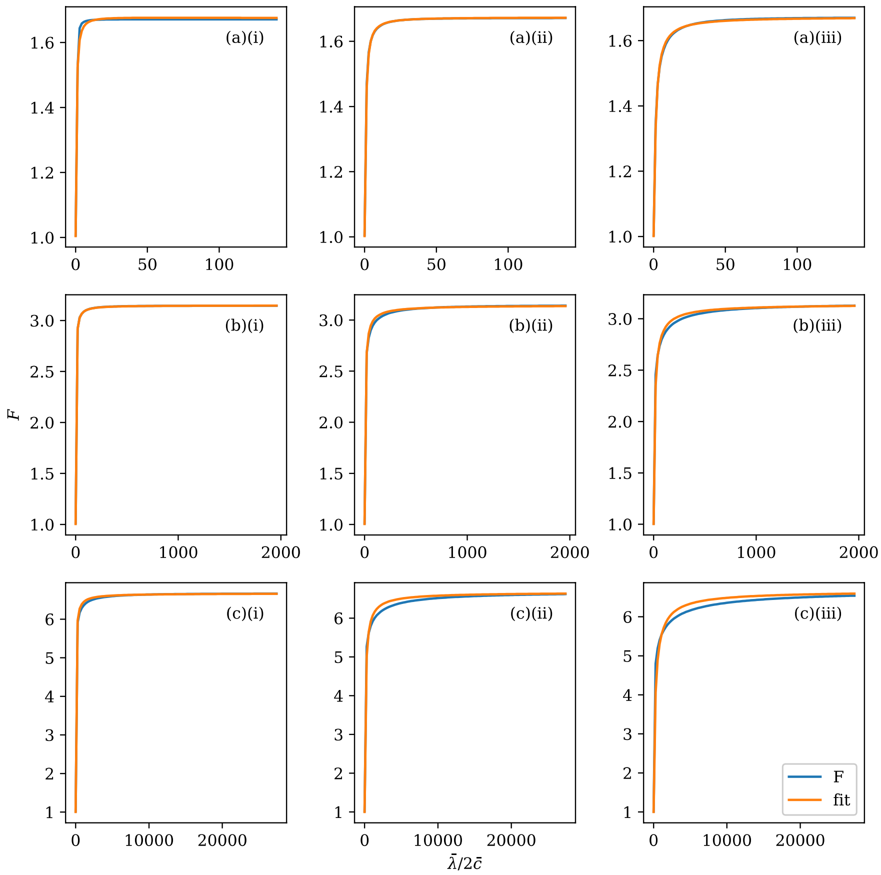

FIGURE 10. Comparisons of the fit function (94) for $F(\bar{\lambda}/2\bar{c},\ \bar{c},\ \rho_0)$ with the numerical results for the gyro-Bohm mode for $\rho_0 = 033$, 0.66 and 1.0, with $\bar{c} =$ 3.438, 6.875 and 10.313. The values of ρ_0 are common in each column and increase from left to right and the values of $\bar{c}$ are common in each row and increase from top to bottom.

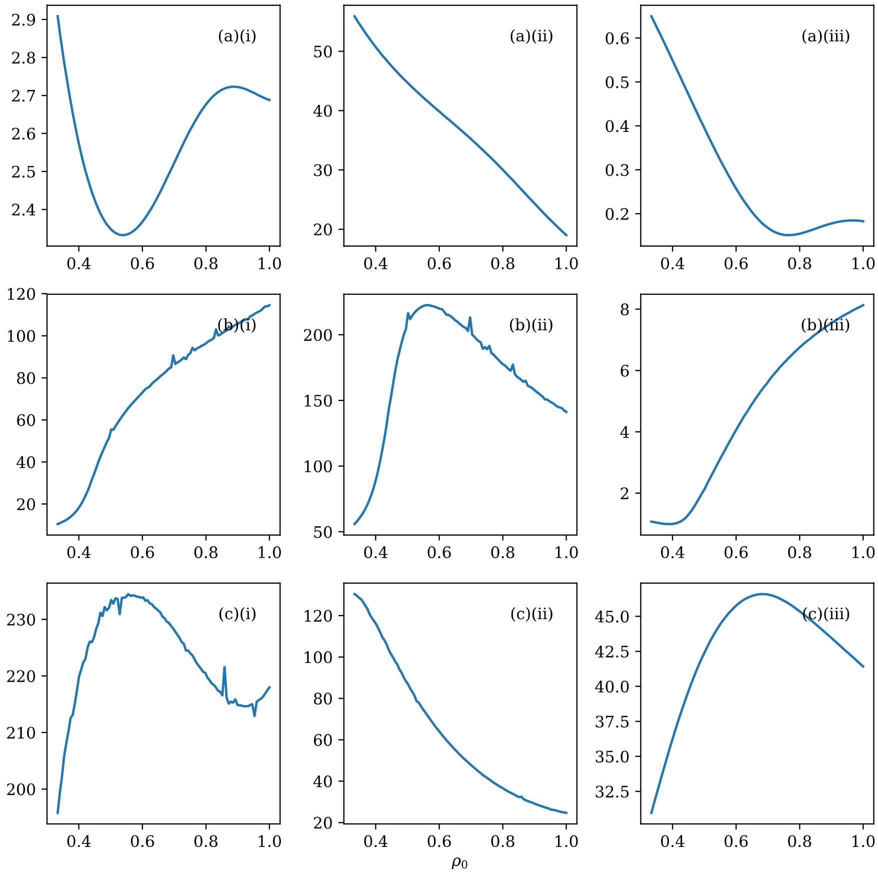

FIGURE 11. The variation of the coefficients a and b used in the fitting function (94) with ρ_0 for $\bar{c} = 3.438$, 6.875 and 10.313. The left-hand column is for a, the middle column for b and the right-hand column shows the mean square error in the fits. The values of $\bar{c}$ are common in each row and increase from top to bottom.

Since $\lambda = \lambda_{\mathrm{H}}(1-\gamma)$, eqn. (95) also shows how impurity radiative losses affect confinement. The resulting confinement time scaling follows from $\hat{\tau}_{\mathrm{E,Rad}} = \mathrm{F}\big(\lambda_{\mathrm{H}}(1-\gamma)\big)/\lambda_{\mathrm{H}}$. This expression could be helpful in DEMO studies [Lux *et a*l., 2015, Lux *et al.*, 2016].

So far, we have emphasized the effect of input power on the scaling of F and $\hat{\tau}_E$, but the dependence on other machine parameters, such as appear in a typical ITER confinement scaling [Doyle *et al.*, 2007] or ST scaling [Buxton *et al.*, 2019], namely magnetic field, B, plasma current, I, R, n, R/a, etc., would follow from introducing such dependencies into the thermal diffusivity at the pedestal top, χ_a. For the gyro-Bohm model one would expect

$$\chi_a \sim \frac{T_a^{3/2}}{B^2 a}\left(\frac{na}{T_a^2}\right)^p f\left(\frac{a}{R}, q \dots\right), \tag{96}$$

where na/T_a^2 represents a possible collisionality dependence, p is some power and f is a function of geometry, such as inverse aspect ratio, a/R, and the safety factor, q [Connor, 1988]. Thus, for given values of W_{Ped} and T_a, geometry and q,

$$\lambda \propto \frac{B^2 a^{3-p}}{n^{1+p}}, \tag{97}$$

which can be introduced into eqn. (95), leading to an additional fitting parameter, p , but covering a range of B, a and n . The results of such extensions could then be compared with global confinement databases [Doyle *et al*., 2007], optimising the choice of the parameters a and b, or relating them to the experimental values of the heating profiles and critical gradients. However, the issue of the pedestal energy remains to be resolved.

To briefly summarise, our principal findings are:

(i) The radial regions that first experience the onset of stiff transport are dependent on the heating profile and transport model and STs are more resilient to this onset occurring.

(ii) The heating power dependence of the plasma energy content that takes account of the gradual onset of stiff transport (from which one can readily deduce the energy confinement) has been calculated.

(iii) An algebraic expression for this power dependence has been developed and it reflects the nature of the heating profile.

(iv) The extent to which impurity radiation losses impact on the energy confinement and modify the scaling law in the presence of stiff transport has been quantified.

This modelling could be improved while still retaining a similar calculation, though at the cost of more algebraic complexity, by (i) allowing an additional radial dependence in the thermal diffusivity, as in the example in the Appendix, and (ii) allowing the impurity radiative loss to occur in a region of different width to that of the heating power, though still assuming both are box-like. Indeed, in the transport code simulations of Fable *et al*., 2019, it was found that the effect of impurity radiation on confinement was most reduced if the heating, due in that case to fusion reactions peaked on axis, was separated from an outer radiating zone. Realistic radial profiles for these quantities could be addressed using the type of modelling presented here, using numerical solutions provided by a transport code. However, the present calculation indicates, by allowing us to study in detail the properties of the analytic solutions, the care needed to monitor where the onset of critical gradients, arises, which we have seen can occur in distinct radial regions of the plasma as the heating profile changes.

One of us, J W C, acknowledges valuable and stimulating discussions with Drs P Buxton, A Costley and S McNamara of Tokamak Energy, who brought this problem to my attention.

REFERENCES

ABRAMOWITZ, M. & STEGUN, I. A., 1972 *Handbook of Mathematical Functions* (New York: National Bureau of Standards, Applied Mathematics) chapter 6.

BRENT, R. P., 1973 *Algorithms for Minimization Without Derivatives* (Englewood Cliffs, NJ: Prentice-Hall) chapter 3-4.

BUXTON, P. F., CONNOR, J. W., COSTLEY, A. E., GRYAZNEVICH, M. P., & MCNAMARA, S. 2019 On the energy confinement in spherical tokamaks: implications for the design of pilot plants and fusion reactors, *Plasma Phys. Control. Fusion*, **61** (3) 035006 (7pp).

CHAPMAN, I. T., SIMPSON, J., SAARELMA, S., KIRK, A., O'GORMAN, T., SCANNELL, R., & THE MAST TEAM 2015 The stabilizing effect of core pressure on the edge pedestal in MAST plasmas, *Nucl. Fusion* **55** (1) 013004 (5pp).

CONNOR, J. W. 1988 Invariance principles and plasma confinement, *Plasma Phys.& Control. Fusion* **30** (6) 619-650.

CONNOR, J. W., TAYLOR, J. B. & TURNER, M. F. 1984 Ideal MHD ballooning instability and scaling law for confinement, *Nucl. Fusion* **24** (12) 642-647.

CONNOR, J. W., HAM, C. J. & HASTIE, R. J. 2016 The effect of plasma beta on high-*n* ballooning stability at low magnetic shear, *Plasma Phys. Control. Fusion* **58** (8) 085002 (9pp).

DIMITS, A. M. ET AL. 2000 Comparisons and physics basis of tokamak transport models and turbulence simulations, *Phys. Plasmas* **7** (3) 969-983.

DOYLE, E. J. ET AL. 2007 Progress in the ITER Physics Basis, Chapter 2: Plasma confinement and transport, *Nucl. Fusion* **47** (6) S1-S414.

FABLE, E., WENNIGER, R. & KEMP, R. 2017 Selected transport studies of a tokamak-based DEMO fusion reactor, *Nucl. Fusion* **57** (2) 022015 (7pp).

ITER PHYSICS EXPERT GROUPS ON CONFINEMENT & CONFINEMENT MODELLING & DATABASE, PLASMA CONFINEMENT & TRANSPORT, 1999 ITER Physics Basis, Chapter 2*: Nucl. Fusion* **39** (12) 2175-2249.

KIRK, A., O'GORMAN, T., SAARELMA S., SCANNELL, R., ET AL., 2009 A comparison of H-mode pedestal characteristics in MAST as a function of magnetic configuration and ELM type, *Plasma Phys. Control. Fusion* **51** (6) 065016 (16pp).

KOTSCHENREUTHER, M., VALANJU, P. M., MAHAJAN, A. M. & WILEY, J. C. 2007 On heat loading, novel divertors and fusion reactors, *Phys. Plasmas* **14** (7) 072502 (25pp).

LUX, H., KEMP, R., WARD, D. J. & SERTOLI, M. 2015 Impurity radiation in DEMO systems modelling, *Fusion Eng. Design* **101** 42-51.

LUX, H., KEMP, R., FABLE, E. & WENNIGER, R. 2016 Radiation and confinement in 0D fusion system codes, *Plasma Phys. Control. Fusion* **58** (7) 075001 (5pp).

MAGGI, C. Studies of the Pedestal Structure in JET with the ITER-Like Wall, *Proc. 26th IAEA Fusion Energy Conf.*, 17-22 Oct 2016, Paper EX/3-3.

OCHOUKOV, R., BOBKHOV, V., ANGIONI, C., BENNERT, DUNNE, M., DUX, R. NOYERDAEME, J.-M., ODSREIĔL, T., PÜTTERNICH, T., REIMHOLD, F. & THE AUG TEAM 2015 Evolution of ELMy H-mode performance in presence of core radiation on ASDEX upgrade, Proc. 42nd EPS Conference on Plasma Physics, P1.131.

SUTTROP, W., KAUFMANN, M., DE BLANCK, H., BRÜSEBAUER, B., et al. 1997 Identification of plasma-edge-related operational regime boundaries and the effect of edge instability on confinement in ASDEX Upgrade, *Plasma Phys. Control. Fusion* **39** (12) 2051-2066.

VIRTANEN, P. ET AL., 2019 SciPy 1.0–Fundamental Algorithms for Scientific Computing in PythoP. *preprint* **arXiv:1907.10121**

WARD, D. J., 2010 The physics of DEMO *Plasma Phys. Control. Fusion* **52** 124033 (12) (12pp).

ZOHM, H., TRÄUBLE, F., BIEL, W. FABLE, E., KEMP, R. LUX, H., SICCINIO, M. & WENNIGER, R. 2017 A stepladder approach to a tokamak fusion power plant, *Nucl. Fusion* **57** (8) 086002 (9pp).

ZOHM, H. 2019 (a) On the use of high magnetic field in reactor grade tokamaks, *J. Fusion Energy* **38** 3-10.

ZOHM, H.2019 (b) On the size of fusion power plants, *Phil. Trans. R. Soc.* **A 377**, No. 2141 20170437 (9pp).

Appendix. Improved gyro-Bohm Transport Model

It is more realistic to supplement the simple gyro-Bohm scaling $\chi \sim \tau^{3/2}$ with an additional, radially increasing factor. We take

$$\chi = \frac{(1+\alpha\varrho^2)}{(1+\alpha)}\chi_a(1+\alpha\varrho^2)\tau^{3/2}, \quad \text{(A.1)}$$

with α an $0(1)$ constant. This change implies that, for most reasonable parameters the onset of stiffness starts from the plasma edge and migrates steadily inwards, as in case (i) studied previously. Thus, this is the situation for $\alpha = 2$ and $\rho_0 > 1/4$ for example.

The analysis proceeds as before, with the transport equation becoming

$$\frac{1}{\rho}\frac{\mathrm{d}}{\mathrm{d}\rho}\left(\rho(1+\alpha\varrho^2)\tau^{3/2}\frac{\mathrm{d}\tau}{\mathrm{d}\rho}\right) = -\frac{\bar{\lambda}(1+\alpha)}{\rho_0^2}, \quad \text{(A.2)}$$

so that we can again solve for $u = \tau^{5/2}/(1+\alpha)$.

Before stiffness sets in, the solution is

$$u = u_0 - \frac{\bar{\lambda}}{4\alpha\rho_0^2}\ln(1+\alpha\varrho^2), \qquad \rho < \rho_0 \quad \text{(A.3)}$$

and

$$u = 1 - \frac{\bar{\lambda}}{4}\ln\left(\frac{\varrho^2(1+\alpha)}{(1+\alpha\varrho^2)}\right), \quad \rho > \rho_0 \quad . \quad \text{(A.4)}$$

Matching eqns. (A.1) and (A.2) at ρ_0 yields

$$u = 1 - \frac{\bar{\lambda}}{4}\left(\ln\left(\frac{\rho_0^2(1+\alpha)}{(1+\alpha\rho_0^2)}\right) + \frac{1}{\alpha\rho_0^2}\ln\left(\frac{(1+\alpha\varrho^2)}{(1+\alpha\rho_0^2)}\right)\right), \quad \rho < \rho_0 \quad \text{(A.5)}$$

As $\bar{\lambda}$ increases, stiffness sets in at $\rho = 1$, when

$$\bar{\lambda} = \bar{\lambda}_{\mathrm{c}}^{(1)} = 2\bar{c}(1+\alpha)\,, \quad \text{(A.6)}$$

when u is given by

$$u = \mathrm{e}^{\bar{c}(1-\rho)} \;;\; 1 > \rho > \rho_1 \qquad , \quad \text{(A.7)}$$

with ρ_1 determined by

$$\bar{\lambda} = 2\bar{c}\rho_1(1+\alpha\rho_1^2)\mathrm{e}^{\bar{c}(1-\rho_1)}\,. \quad \text{(A.8)}$$

Then, for $\rho_0 < \rho < \rho_1$,

$$u = \mathrm{e}^{\bar{c}(1-\rho_1)} - \frac{\bar{\lambda}}{4}\ln\left(\frac{\varrho^2(1+\alpha\rho_1^2)}{\rho_1^2(1+\alpha\varrho^2)}\right) \quad \text{(A.9)}$$

and, for $\rho < \rho_0$,

$$u = \mathrm{e}^{\bar{c}(1-\rho_1)} - \frac{\bar{\lambda}}{4}\left(\ln\left(\frac{\rho_0^2(1+\alpha\rho_1^2)}{\rho_1^2(1+\alpha\rho_0^2)}\right) + \frac{1}{\alpha\rho_0^2}\ln\left(\frac{(1+\alpha\varrho^2)}{(1+\alpha\rho_0^2)}\right)\right). \quad \text{(A.10)}$$

When $\rho_1 < \rho_0$, which occurs when

$$\bar{\lambda} = \bar{\lambda}_{\mathrm{c}}^{(2)} = 2\bar{c}\rho_0(1+\alpha\rho_0^2)\mathrm{e}^{\bar{c}(1-\rho_0)}, \tag{A.11}$$

we have

$$u = \mathrm{e}^{\bar{c}(1-\rho)}; \qquad \rho_1 < \rho < 1 \tag{A.12}$$

and

$$u = \mathrm{e}^{\bar{c}(1-\rho_1)} - \frac{\bar{\lambda}}{4\alpha\rho_0^2}\ln\left(\frac{(1+\alpha\varrho^2)}{(1+\alpha\rho_1^2)}\right);\ \rho < \rho_1, \tag{A.13}$$

where ρ_1 is now determined by

$$\bar{\lambda}\frac{\rho_1}{\rho_0} = 2\bar{c}\rho_0(1+\alpha\rho_1^2)\mathrm{e}^{\bar{c}(1-\rho_1)} \quad . \tag{A.14}$$

These expressions can be used to construct

$$F = 2(1+\alpha)^{2/5}\int_0^1 \rho u^{2/5}(\rho)\mathrm{d}\rho \ , \tag{A.15}$$

which involves integrals of the type

$$\hat{F}_1\left(\rho_j, u_0\, , \alpha, \frac{\bar{\lambda}}{4\alpha\rho_0^2}\right) = \frac{(1+\alpha)^{2/5}u_0^{2/5}}{\alpha}\int_1^{1+\alpha\rho_j^2}\left(1 - \frac{\bar{\lambda}}{4\alpha\rho_0^2 u_0}\ln y\right)^{2/5}\mathrm{d}y \ \ \frac{1}{\alpha}\left(\frac{(1+\alpha)\bar{\lambda}}{4\alpha\rho_0^2}\right)^{2/5}\exp\left(\frac{4\alpha\rho_0^2 u_0}{\bar{\lambda}}\right)\left[\Gamma\left(\frac{7}{5}, \frac{4\alpha\rho_0^2 u_0}{\bar{\lambda}} - \ln(1+\alpha\rho_j^2)\right) - \Gamma\left(\frac{7}{5}, \frac{4\alpha\rho_0^2 u_0}{\bar{\lambda}}\right)\right], \tag{A.16}$$

$$\hat{F}_2\left(\rho_j, \rho_k, u_1, \alpha\, , \frac{\bar{\lambda}}{4}\right) = (1+\alpha)^{7/5}u_1^{\frac{2}{5}}\int_{\frac{\rho_j^2(1+\alpha)}{(1+\alpha\rho_j^2)}}^{\frac{\rho_k^2(1+\alpha)}{(1+\alpha\rho_k^2)}}\frac{\mathrm{d}y}{(1+\alpha-\alpha y)^2}\left(1 - \frac{\bar{\lambda}}{4u_1}\ \ln y\right)^{\frac{2}{5}} \quad , \tag{A.17}$$

which needs numerical integration and, as before,

$$F_3(\rho_j, \rho_k) = \frac{2}{\hat{c}^2}\left[(1+\hat{c}\rho_j)\mathrm{e}^{\hat{c}\,(1-\rho_j)} - (1+\hat{c}\rho_k)\mathrm{e}^{\hat{c}\,(1-\rho_k)}\right], \tag{A.18}$$

where we emphasize $\hat{c}$, rather than $\bar{c}$, re-appears. Thus, we obtain for $\bar{\lambda} < \bar{\lambda}_{\mathrm{c}}^{(1)}$

$$F = \hat{F}_1\left(\rho_0, 1 - \frac{\bar{\lambda}}{4}\left[\ln\left(\frac{\rho_0^2(1+\alpha)}{(1+\alpha\rho_0^2)}\right) - \frac{1}{\alpha\rho_0^2}\ln(1+\alpha\rho_0^2)\right], \alpha, \frac{\bar{\lambda}}{4\alpha\rho_0^2}\right) + \hat{F}_2\left(\rho_0, 1, 1 - \frac{\bar{\lambda}}{4}\ln(1+\alpha), \alpha, \frac{\bar{\lambda}}{4}\right). \quad \text{(A.19)}$$

For $\bar{\lambda}_\mathrm{c}^{(1)} < \bar{\lambda} < \bar{\lambda}_\mathrm{c}^{(2)}$

$$F = \hat{F}_1\left(\rho_0, e^{\bar{c}(1-\rho_1)} - \frac{\bar{\lambda}}{4}\left(\ln\left(\frac{\rho_0^2(1+\alpha\rho_1^2)}{\rho_1^2(1+\alpha\rho_0^2)}\right) - \frac{1}{\alpha\rho_0^2}\ln\big((1+\alpha\rho_0^2)\big)\right), \alpha, \frac{\bar{\lambda}}{4\alpha\rho_0^2}\right) + \hat{F}_2\left(\rho_0, \rho_1, \mathrm{e}^{\bar{c}(1-\rho_1)} - \frac{\bar{\lambda}}{4}\ln\left(\frac{(1+\alpha\rho_1^2)}{\rho_1^2}\right), \alpha, \frac{\bar{\lambda}}{4}\right) + F_3(\rho_1, 1). \quad \text{(A.20)}$$

Finally, for $\bar{\lambda} > \bar{\lambda}_\mathrm{c}^{(2)}$,

$$F = \hat{F}_1\left(\rho_1, \mathrm{e}^{\bar{c}(1-\rho_1)} + \frac{\bar{\lambda}}{4\alpha\rho_0^2}\ln\big((1+\alpha\rho_1^2)\big), \alpha, \frac{\bar{\lambda}}{4\alpha\rho_0^2}\right) + F_3(\rho_1, 1). \quad \text{(A.21)}$$

However, given that $\hat{F}_2$ needs to be evaluated numerically, it is more straightforward to evaluate F directly from eqn. (A.15) using the appropriate expressions for $u(\rho)$.